# Journal of EARTH Science and Engineering

ISSN 2159-581X

Volume 4, Number 2, February 2014

# Journal of Earth Science and Engineering

Volume 4, Number 2, February 2014 (Serial Number 29)

David Publishing Company
www.davidpublishing.com

**Publication Information:**
*Journal of Earth Science and Engineering* is published monthly in hard copy (ISSN 2159-581X) by David Publishing Company located at 240 Nagle Avenue #15C, New York, NY 10034, USA.

**Aims and Scope:**
*Journal of Earth Science and Engineering*, a monthly professional academic journal, covers all sorts of researches on (but not limited to): Physical Geography (Soil Science and Remote Sensing), Geology, Geophysics, Geochemistry, Geobiology, Atmospheric Science, Marine Science and Space Physics, etc..



Manuscripts and correspondence are invited for publication. You can submit your papers via Web Submission, or E-mail to earth@davidpublishing.org, info@davidpublishing.org or earth_science2011@hotmail.com. Submission guidelines and Web Submission system are available at http://www.davidpublishing.com, http://www.davidpublishing.org.

**Editorial Office:**
240 Nagle Avenue #15C, New York, NY 10034, USA
Tel: 1-323-984-7526, 323-410-1082
Fax: 1-323-984-7374, 323-908-0457
E-mail: earth@davidpublishing.org; info@davidpublishing.org; earth_science2011@hotmail.com.



**Abstracted/Indexed in:**
Database of EBSCO, Massachusetts, USA
Chinese Database of CEPS, Airiti Inc. & OCLC
Cambridge Science Abstracts (CSA)
Ulrich's Periodicals Directory
Summon Serials Solutions
Proquest

**Subscription Information:**
Price (per year):
Print $420, Online $300
Print and Online $560

David Publishing Company
240 Nagle Avenue #15C, New York, NY 10034, USA
Tel: 1-323-984-7526, 323-410-1082; Fax: 1-323-984-7374, 323-908-0457
E-mail: order@davidpublishing.com

DAVID PUBLISHING

David Publishing Company
www.davidpublishing.com

Journal of Earth Science and Engineering

Volume 4, Number 2, February 2014 (Serial Number 29)

# Contents

Journal of Earth Science and Engineering 4 (2014) 73-79

# Development of a Cooling System for Geothermal Borehole Probes

Benedict Holbein and Joerg Isele

*Geothermal Group of the IAI (Institute for Applied Computer Science), KIT (Karlsruhe Institute of Technology), Karlsruhe 76344, Germany*

Received: November 28, 2013 / Accepted: January 12, 2014 / Published: February 25, 2014.

**Abstract:** The high potential of geothermal energy in quantity and availability can be a great option, facing the huge problem of growing energy use linked with the climatic problems. Therefore, it is necessary to reduce costs and risks for the use of geothermal energy sources. Because most of the problems have to do with insufficient knowledge about the conditions in the earth crust, the key to take root of geothermal energy is widespread research. The cooling system allows the use of all needed devices in deep boreholes without strict time or temperature limitations, which promotes the achieving of comprehensive information. To develop the purpose-built components among conducting experiments about the thermodynamic processes, a prototype is provided step by step.

**Key words:** Monitoring, heat protection, borehole tools, engineering.

## 1. Introduction

Borehole temperature in Germany normally does not exceed 200 °C but there exists geothermal locations with much higher temperatures. There are intentions to use the heat of magma chambers [1]. Because only a few electronic components and special seal materials withstand temperatures around 200 °C, logging in these boreholes is already a serious problem. Therefore, it would be a great advance to introduce an active cooling system for logging devices with unlimited operating time.

## 2. The System

The cooling system shall make it possible to use various measurement devices with standard electronics for long time periods, in boreholes with temperatures up to several hundred degrees Celsius. Therefore, the concept [2] consists of two central fields. The first one is the insulation to reduce the heat input from outside. The second field of the concept is a thermodynamic cycle process to limit the temperature inside the cool room (Fig. 1).

### 2.1 Insulation

A MLI (multi layer insulation) and a vacuum-insulation inside the wall of the refrigeration room housing minimize heat radiation and heat conduction at ones. The first experiments show that the heating-up of the refrigeration room is slowed down significantly with a vacuum of less than 0.5E-4 mbar (Fig. 2).

For the corresponding experiment, a heating jacket is used to heat the cool room from outside. The temperature profiles inside are logged during different runs, with or without vacuum and compared afterwards. The results show clearly that the vacuum insulation works, though there are still some technical problems with its stability.

### 2.2 Active Cooling

The heat which gets through the insulations and the

**Corresponding author:** Benedict Holbein, B.Sc., research fields: mechanical-engineering and thermodynamics. E-mail: benedict.holbein@kit.edu.

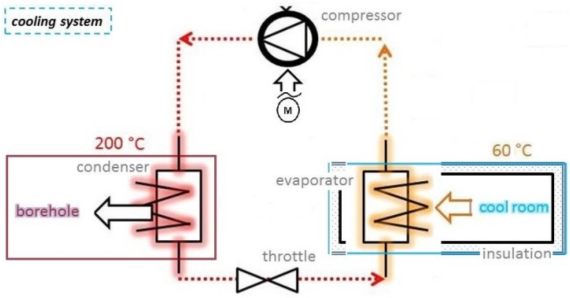


**Fig.1 Cooling system concept.**

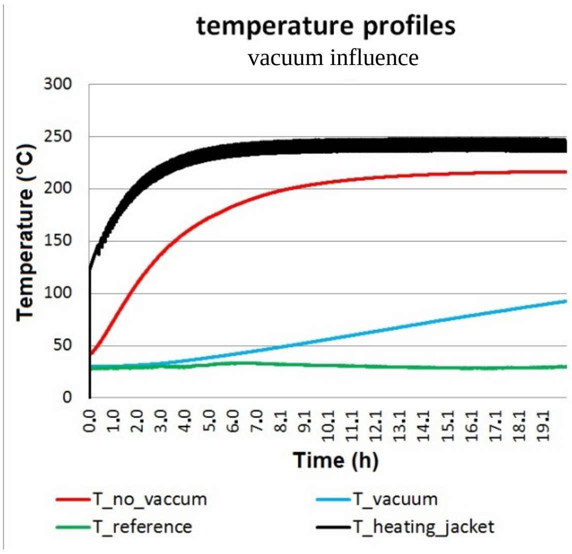


**Fig. 2 Influence of vacuum insulation.**

heat produced by the electronic components themselves have to be dissipated to guarantee that a maximum temperature of 70 °C will not be exceeded. This prevents damage to the components by overheating. If the devices are realized, appending electronics can be used without time limitations, like it would exist using only PCM (phase change material) cooling. The process consists of four important sub-processes, which have to be carried out by purpose-built components.

### *2.3 The Process*

The special ambient conditions in the boreholes evoke a special process conduct (Table 1 and Fig. 3). This means that usual refrigerants are not usable. Searches for compounds with fitting evaporation temperatures and pressures indicated acetone, 1.1-dichlorethane and ethyl-formate as possible refrigerants for 200 °C environments. In the moment acetone is preferred, because it is the best known and available substance of the mentioned fluids. Fig. 3 shows the predicted process with acetone in a borehole with 200 °C ambient temperature [3].

For hotter surrounding, it is possible to use a 2nd stage with a 2nd refrigerant, whose intermediate cool room serves as the surrounding for the first stage condenser. Following an analogical structure as in stage one, the 2nd refrigerant evaporates in the intermediate cool room, becomes compressed gaseous and condenses above the ambient temperature of the borehole. The whole system can be imagined as a refrigerator inside a house with air conditioner, but with very different temperatures. An example for the 2nd stage with dodecane is pictured in Fig. 4.

The maximum cooling capacity can be calculated as follows [4].

$$\frac{dQ}{dt} = \dot{m} \times T_1 \times (s_1 - s_4)$$
$$\cong \dot{m} \times \left[\frac{dp}{dT} \times T_1 \times x \times (v'' - v')\right]$$
$$\cong \dot{m} \times \left[\frac{dp}{dT} \times T_1 \times x \times (v'' - v')\right] \quad (1)$$

where,

$\mathrm{d}Q$: Heat differential;
$\mathrm{d}p$: Pressure differential;
$\mathrm{d}T$: Temperature differential;
$\mathrm{d}t$: Time differential;
$\dot{m}$: Mass flow;
$T$: Temperature;
$s$: Entropy;
$x$: Percentage of liquid phase;
$v''$: Specific volume superheated;
$v'$: Specific volume sub cooled.

## 3. The Components

The extreme process and environment conditions, corrosive surrounding media and aggressive refrigerants pose a big challenge for the engineering of the cooling system components. Besides, the probe has to be designed compactly.

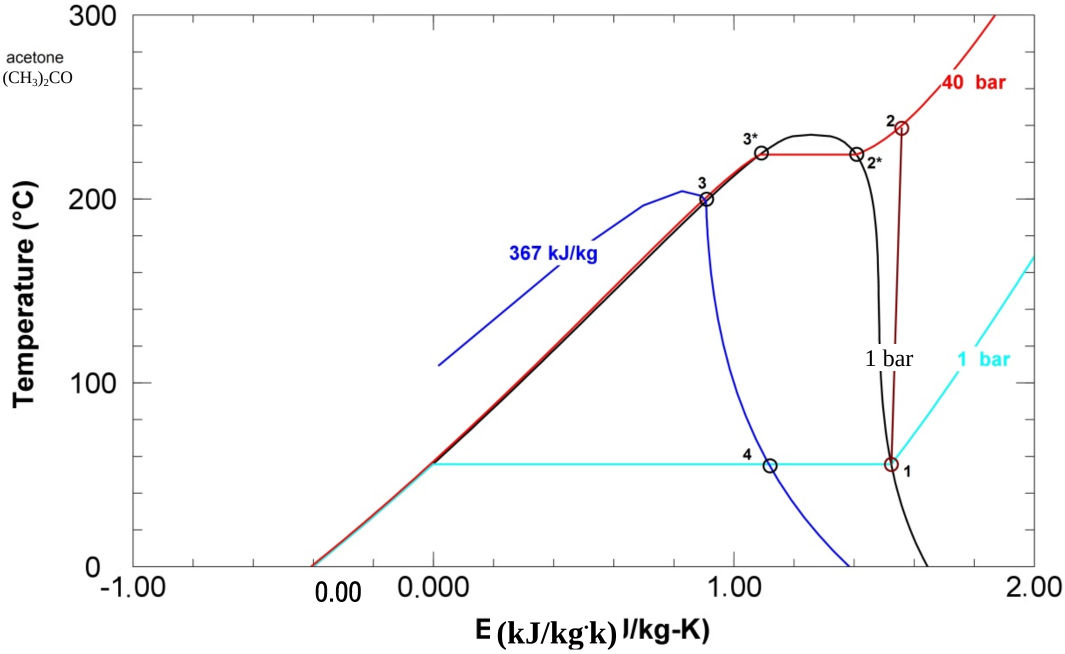


**Fig. 3 Acetone cooling process.**

**Table 1 Sub-processe**

| Diagram | Conditions | Sub process |
|---|---|---|
| 4-1 | 56.5 °C, 1 bar | Isothermal evaporation |
| 1-2 | Gaseous | Polytropic compression |
| 2-2* | Isobar | Sensible heat loss |
| 2*-3* | 220 °C, 40 bar | Isothermal condensation |
| 3*-3 | Isobar | Sensible heat loss |
| 3-4 | | Isenthalpic expansion |

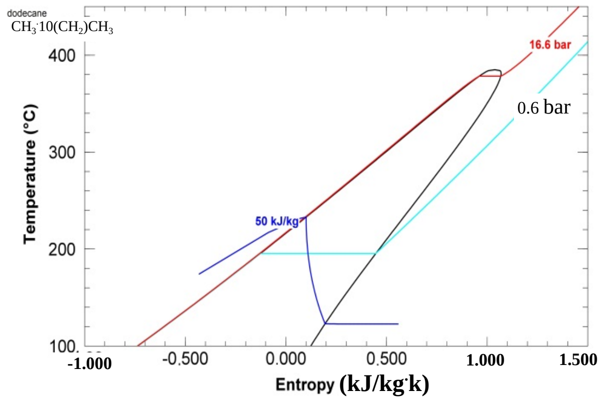


**Fig. 4 2nd stage: dodecane.**

To be usable in most of the boreholes, the outer diameter should not exceed 170 mm. Because the evaporator has to fit into the cool room, this means that the actual diameter's maximum is 110 mm. In future probe deigns, diameters of 129 mm will be allowed for the evaporator. It has to be mentioned that the components which have to be cooled have to fit in the cool room as well.

The prototype currently used for the experiments was engineered with the aim to achieve maximum surface for heat conduction under the constraint of available space in the cool room (Fig. 5).

The condenser is in preparation for TUV (Technical Control Board), because it needs a technical approval for inside pressures of over 40 bar. The throttle and the compressor are in the construction design phase. The assembly of a big compressor for the usage in laboratory experiments is running. The condenser can take more space as the evaporator placed outside, but has direct contact with the borehole environment. It has to resist the high temperatures and pressures and still perform a sufficient heat transfer.

Materials which are usable for this purpose, like nickel-base alloys, are expensive and difficult-to-machine. To reach a big surface for heat conduction, the design is based on a small tube structure (Fig. 6).

**Fig. 5 Evaporator.**

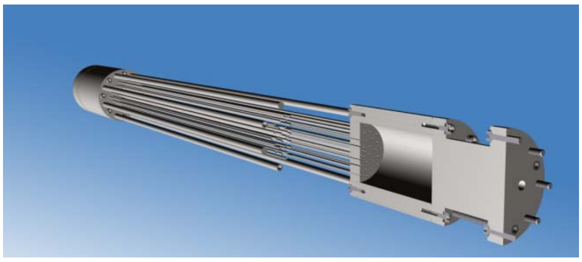

**Fig. 6 Condenser engineering model.**

## 4. Problems

The installation space, operating temperatures and pressures can be summarized as inner problems for the cooling system. As outer problems, the ambient temperatures, pressures and corrosive media have to be mentioned. A big issue for the system which occurs inside and outside the system, even though with different parameters, is the heat conduction. Talking about insulation, some possibilities to minimize the heat conduction were described.

In contrast to this, the condensation and evaporation process require good heat conduction performances. In Eq. (2) the most important influencing variables can be recognized [5]. The heat transfer coefficients $\alpha_i$ depend on involved materials and fluids and like the temperature gradient $\Delta T$ , also on constant process parameters. Hence they are only partly modifiable and the surface $A$ has to be focused to increase the transferable heat flow $\mathrm{d}Q/\mathrm{d}t$.

$$\frac{\mathrm{d}Q}{\mathrm{d}t} = \left(\sum_{i=1}^{n} \alpha_i\right)^{-1} \times A \times \Delta T \quad (2)$$

Because there are many heat transfer steps (Fig. 7), the heat conduction issue is very complex. It is nearly impossible to implement simulations which can deliver reliable prognoses, without trustable validation by several experiments.

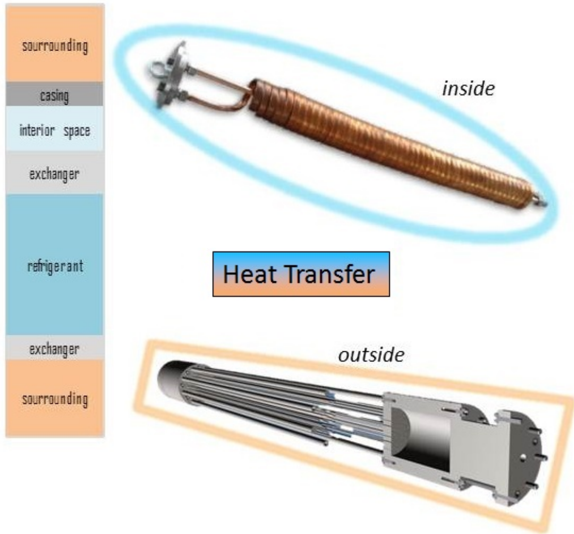


**Fig. 7 Heat transfer steps.**

That is why experiments are central tasks during the development of the cooling system for the validation of the constructed component prototypes and the prognosticated process behavior.

## 5. Experiments

### *5.1 Evaporation and Heat Transfer*

(1) Outer heat source: Following the process structure, the first sub-process to investigate is the evaporation. Using acetone as refrigerant and a prototype of the refrigeration room housing (with integrated MLI and vacuum insulation of < 0.5E-4 mbar) the cooling and heat transfer capacity is tested. The latest evaporator version (Fig. 5) was utilized as a heat exchanger inside. The casing is heated up from outside with a heating jacket at over 200 °C (Fig. 8).

The evaporator is filled with 700 mL of liquid acetone at atmospheric pressure. With thermocouples inserted in the casing and the evaporator, the temperature-time curves are plotted (Fig. 9).

The profile shows a temperature plateau at 56.5 °C for about 200 min, which indicates the evaporation phase. With Eq. (1) and the substance properties of

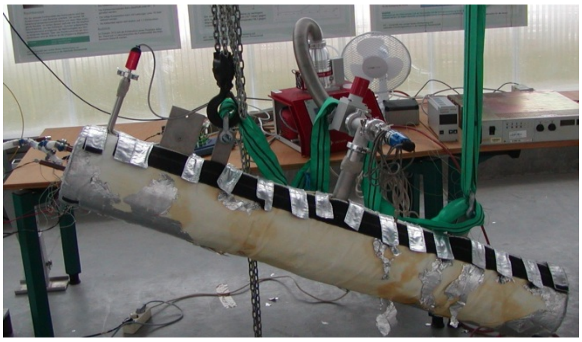

Fig. 8 Cool room casing with heating jacket.

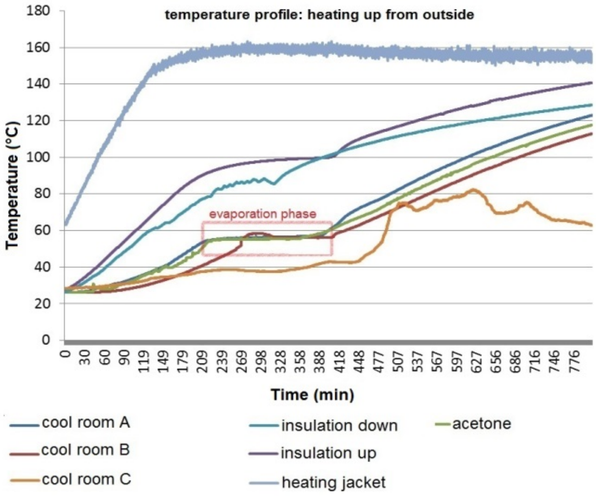


Fig. 9 Temperature profile, outer heat source.

acetone, the cooling capacity is estimated (Table 2). The result is about 22 Watt, which is equivalent with the heat flow from outside through the insulation. The temperature curves of the air and acetone do not differ much. The temperature inside the insulation layers of ceramic wool at the casing bottom and cover runs at a significant higher level, because there is no MLI and vacuum insulation in axial direction.

(2) Outer and inner heat sources: In the next step a board with resistors is installed additionally, to simulate the loads in the cool room. A part of them is admitted with output of 20 Watt, the rest stay dead (Fig. 10). So in total (with heating jacket outside) there is a heat input of about 40 Watt inside the casing.

The temperature profiles are logged with the same quantity of acetone (700 mL) as before (Fig. 11).

The problem which occurs is that the resistors heat up to fast in comparison with the acetone. That is why

Table 2 Substance properties of acetone.

| $m$ (kg) | Time (s) | $s_1$ (kJ/kg·K) | $s_4$ (kJ/kg·K) | $T_1$ (K) | Cooling capacity (W) |
|---|---|---|---|---|---|
| 524E-3 | 12E+3 | 1.525 | -5E-4 | 329.5 | 21.95 |

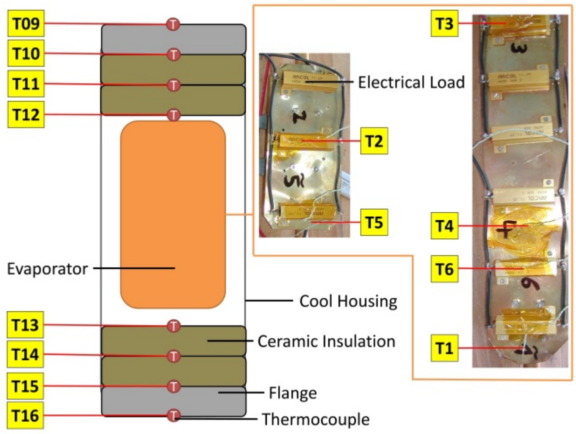


Fig. 10 Thermocouples and resistors.

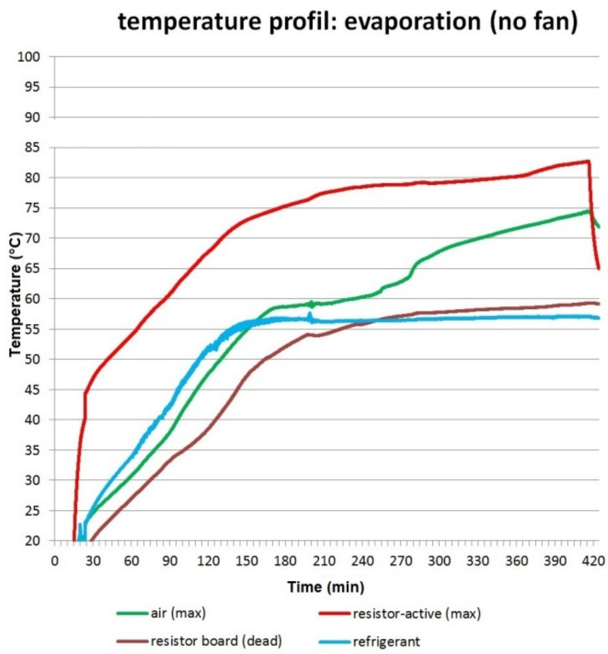


Fig. 11 Temperatures, inner and outer heat source.

the plateau is reached when the temperatures are above 70 °C. For the electronics in the later probe this would mean damage which has to be prevented. The results show that the heat conduction from the loads to the refrigerant has to be optimized. A simulation shows that forced convection of the inner air would improve the problematic heat transfer (Fig. 12).

In the first test a fan was used to move the air inside the cool room (Fig. 13).

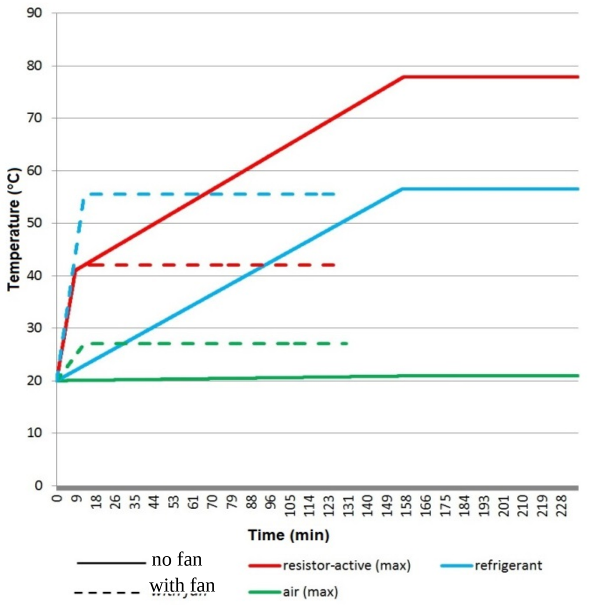


Fig. 12 Simulation of temperature profiles.

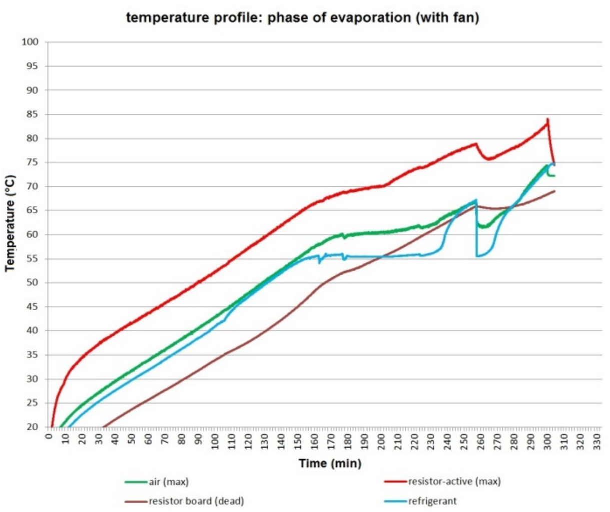


Fig. 13 Temperature profiles with fan.

As a result, the temperature gradient between refrigerant and resistors is smaller and the resistors heat up slower. But the temperature profiles logged deviate notable from the simulation prognosis and the improvement of the heat transfer is weaker as expected and not sufficient for later application.

*5.2 Optimization*

A new evaporator design shall make the problematic heat transfer more direct. Besides it can perform a higher refrigeration capacity and offers more installation surface for loads (Fig. 14).

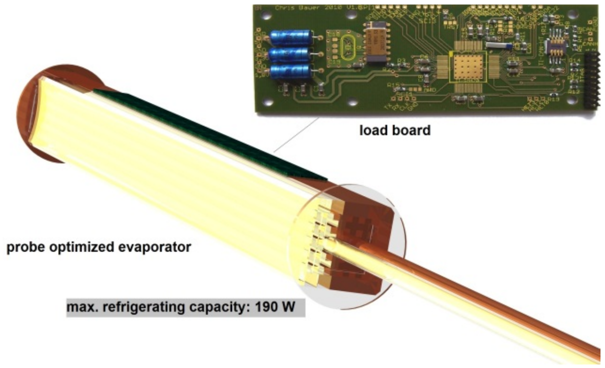


Fig. 14 Probe optimized evaporator.

Accordingly, the other components, like condenser and compressor, have to be tested under realistic conditions in the laboratory. Based on the experiments, they can be optimized in a 2nd iteration step. Following this structure, it is possible to approximate an optimal cooling cycle and to realize a solid construction simultaneously. The end of this described operating sequence will be an operational prototype, which can be varied and rapidly adjusted.

## 6. Prospects

*6.1 Next Steps*

There is still a lot of work to do, realizing a complete prototype of the borehole cooling system. After testing the evaporation phase firstly, there have to follow more experiments to optimize this sub-process. The next step to do is the installation of experiments for the missing sub-processes condensation, compression and expansion and to combine them to form the whole cooling cycle in the laboratory, which shall be realized within this year.

Therefore, the component prototypes for compressor, throttle and condenser are in preparation.

*6.2 Open Questions*

Besides the concrete steps for the development of a prototype of the cooling systems, questions about field operation and special applications have to be answered. The engineering of components like the compressor and the implementation of experiments are expensive and time-consuming.

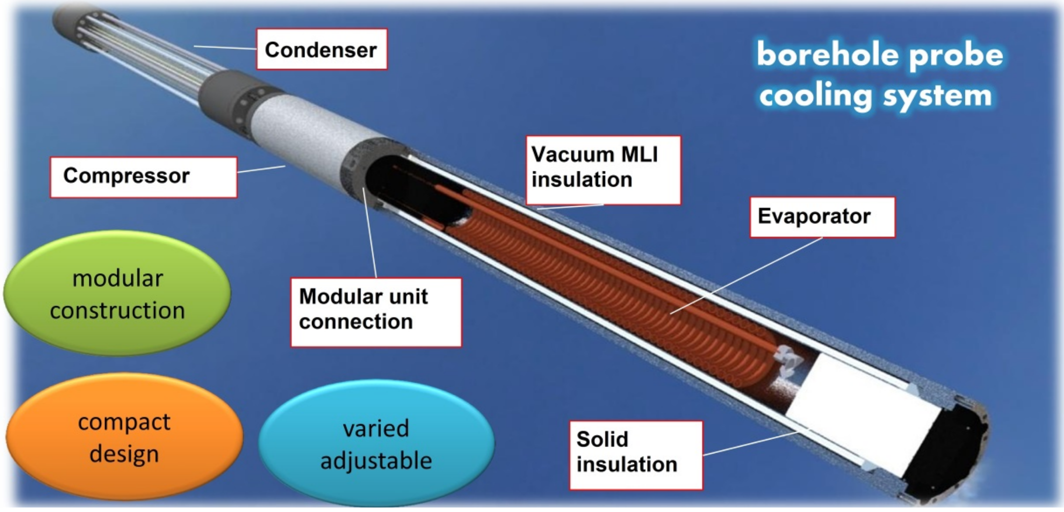


**Fig. 15 Model of the borehole cooling system.**

Even if a usable machine will stay at the end of this project, it is still a research project which first and foremost aims at scientific findings and is shareware oriented. That simplifies some engineering exercises, relieving them from economic factors, but on the other hand brings difficulties for the financing. For further development and a better performance, it could be reasonable to find partners for technical parts, as well as for questions about application.

A vision for a possible version of the borehole cooling system has already existed (Fig. 15).

## References


[1] High Temperature Downhole Tools—Recommendations for Enhanced and Supercritical Geothermal Systems, White Paper, IPGT (International Partnership of Geothermal Technology), 2012.

[2] B. Holbein, Entwicklungeines Kühlsystemsfür Geothermie Bohrlochsonden (Development of a cooling-system for geothermal borehole tools), Bachelor Thesis, Karlsruhe Institute of Technology, Karlsruhe, Germany, 2011.

[3] Reference Fluid Thermodynamic and Transport Properties—REFPROP, Version 9.1, Applied Chemicals and Materials Division, NIST (National Institute of Standards and Technology), Boulder, Colorado, 2013.

[4] Wärmeatlas, VDI (Verein Deutscher Ingenieure), VDI-GVC (Gesellschaft Verfahrenstechnik und Chemieingeniuerwesen), (Society of German Engineers, Process Technology and Chemical Engineering Springer), Heidelberg, Germany, 2009.

[5] F. Brandt, Wärmeübertragung in Dampferzeugern und Wärmetauschern (Heat-Transfer in Evaporators and Heat-Exchangers), FDBR—Association of Steam Boiler, Pressure Vessel and Piping Manufacturers, Vol. 2, Vulkan-Verlag, Essen, 1995, pp. 45-50, 74-80.

Journal of Earth Science and Engineering 4 (2014) 80-87

# Grain Size and Metallic Trace Element Contents in Sediments of Kemaman Coast, Terengganu, Malaysia, South China Sea

Nor Antonina Abdullah[1], Noor Azhar Mohd Shazili[1], Rosnan Yaacob[1] and Kamaruzzaman Yunus[2]

*1. School of Marine Science and Environment, University Malaysia Terengganu, Kuala Terengganu 21030, Malaysia*

*2. Bandar Indera Mahkota, University Islam Antarabangsa Malaysia, Kuantan 25200, Kuala Terengganu, Pahang,* Malaysia

Received: December 19, 2013 / Accepted: January 16, 2014 / Published: February 25, 2014.

**Abstract:** A total of 43 sediment samples were collected at Kemaman coast, Terengganu, by using Smith McIntyre grab. These sediments were analyzed to determine the grain size, sediment texture and metallic trace elements. Lazer diffraction method using PSA (particle size analyzer) was used to determine the grain size and sediment texture. Teflon bomb was used to digest the sediments for metallic trace elements concentration. Results showed that the study area was dominated with sand particles (60.5%) followed by loamy sand (20.9%), sandy clay (16.3%) and silt loam (2.3%). On the other hand, the average concentrations of each metallic trace elements were 0.12 μg/g for Cd; 36.6 μg/g for Cr; 9.51 μg/g for Cu; 11.6 μg/g for N: 41.5 μg/g for Zn and 29.3 μg/g for Pb. Based on the results, it was found out that coarse sediments showed lower levels of metallic trace elements and higher levels in fine sediments. In addition, enrichment factor was calculated to assess the pollution status of the study area. Based on the calculation, the enrichment of metallic trace elements ranked in the following order: Pb > Cd > Zn > Cu > Ni > Cr. The significant enrichment of Pb and moderate enrichment of Cd and Zn indicated that there are anthropogenic inputs while the rest of the metals can be considered from natural sources although there are effects of anthropogenic inputs in some sampling location.

**Key words:** Sediment, Kemaman coast, metallic trace elements.

## 1. Introduction

Sediments act as one of the ultimate sinks for trace metal inputs into the aquatic environment hence, they cannot fix metals permanently. Some of the sediment bound metals might be released into the water body through various processes of remobilization under variable conditions. In this aspect, sediments are the main repository and source of trace metals in the marine environment and play an important role in the transport and storage of potentially hazardous metals. Sediments also act as scavengers for trace metals and often provide an excellent proof of man's impact [1]. To some extent, trace metals in sediments can reflect the quality of the water body. Sediment analysis is a common tool to determine the index of pollution of drainage basins because of the tendency of pollutants to accumulate in the sediments. The living community associated with sediments is particularly prone to harmful effects of pollution [2].

Trace metals are considered very important and highly toxic pollutants to various environments and to some extent under certain circumstances can be further transformed into more toxic compounds [3]. Trace metals are of considerable environmental concern due to their toxicity, wide sources, non-biodegradable properties and accumulative behaviors. The input of trace metals into marine environment poses danger to the aquatic organisms especially the sediment associated organisms. This in

**Corresponding author:** Nor Antonina Abdullah, Ph.D., research fields: sedimentology, mineralogy and marine pollution. E-mail: antonina@umt.edu.my.

turn will affect the health of human who consume living organisms which accumulate trace metals.

## 2. Materials and Methods

### *2.1 Description of the Study Area*

Kalong Bay is an industrial area of Kemaman district. Currently, the Kuantan Port Consortium Sdn Bhd is operating Kemaman Port's 510 m long West Wharf in this area (Kuantan Port Consortium Sdn Bhd, 2013). The following are the categories of ships which are anchored in the study area (Ports World Sdn Bhd, 2000) such as, deep Water Anchorage, Quarantine Anchorage, Explosive Anchorage and Tanker Anchorage.

### *2.2 Sampling and Sample Preparation*

Surface sediment samples were collected from 43 stations using the Smith McIntyre grabs on board DISCOVERY I from July 15-18, 2012. The sediments were taken from the middle of the grab using plastic scope and put in labeled plastic bags. The sediments were put in the ice box and kept frozen then brought back to the laboratory for analysis. The sediment samples were even dried at 150 ºC for 7 h then lightly ground to break up the particles and sieved using less than 63 µm mesh sieve. The samples were kept in a cleaned polyethylene bottles for trace metal contents by using ICP-MS (inductively coupled plasma mass spectroscopy) model Perkin-Elmer 2000.

## 3. Analytical Techniques

### *3.1 Grain Size Analysis*

For grain size, approximately 5 g of sediment samples were used then 5 mL of Calgon solution was added overnight to the sample to disperse the sediments. After mixed the samples were injected to the Particle Size Analyzer Mastersizer 2000. The data obtained were used to calculate the grain size (mean size, sorting and skewness) through Microsoft excel and the sand, silt and clay to determine the textural classes of the sediments using USDA (United States Department of Agriculture) soil textural triangle.

### *3.2 Trace Metallic Elements*

3.2.1 Microwave Digestion

The sediment samples were digested for metallic trace element contents by following standard methodologies with some modifications [4]. The digestion procedure involved heating 0.05 g sediment sample in a sealed Teflon vessel with a 1.5 mL mixed acid solution of concentrated $HNO_3$, HCl and HF with 3:3:1 ratio. The vessel was heated at 150 °C for 7 h. After room temperature was cooled, the digested sample was transferred into 15 mL centrifuge tube and diluted to 10 mL with ultra-pure water. For the validation method, certified reference material NBS 1646a estuarine sediment was analyzed and digested to determine the recovery levels and accuracy of metallic trace element analysis. Table 1 shows the recoveries for all metallic trace elements, ranged between 91.08%-125% with slightly higher recoveries obtained for Pb. Metallic trace elements were analyzed using ICP-MS.

3.2.2 EF (Enrichment Factor)

The EF was calculated to determine the presence of anthropogenic sources in the sediments. The calculation included normalization by the aluminium contents. The EF of the metallic trace elements was calculated using the following formula:

$$EF = (E/Al)\ sed.\ /(E/Al)\ ucc \quad (1)$$

where, (E/Al) sed. denotes the levels of metallic trace elements in the sediment sample and (E/Al) ucc

**Table 1 Results of analyses of certified reference materials (NBS 1646a Estuarine Sediment).**

| | Certified value (µg/g) | Measured value (µg/g) | Mean recovery (%) |
|---|---|---|---|
| Chromium | 40.9 | 40.06 | 99.27 |
| Nikel | 23 | 22.82 | 99.22 |
| Copper | 10.01 | 9.83 | 98.22 |
| Zinc | 48.9 | 47.10 | 96.32 |
| Cadmium | 0.148 | 0.13 | 91.08 |
| Lead | 11.7 | 14.66 | 125.3 |

denotes the levels of metallic trace elements from UCC (upper continental crust) [5]. EF > 1.0 indicates an enrichment or pollution by the elements. Fig. 1 shows the location of stations in the study area.

## 4. Results and Discussion

Sediments in the South China Sea may be classified into six grain size types: gravelly sand, sand gravel, sand, clayey silt, silt clay and clay. The grain size of the sediments plays an important role in controlling the contents of the elements. Average contents of most elements increase with the decrease of grain size. The enrichment of elements in fine-grained sediments is attributable to their high adsorption capacity, high abundance in organic matter and low contents of quartz.

Table 2 shows the results of grain size of the sediments in the study area. Mean size indicates the strength of water movement which supplies detrital materials to the site of sedimentation. The average mean size of sediment is 3.48Ø (very fine sand) which ranged from 2.18-5.49Ø. The highest mean size is observed at station 5 (5.50Ø, medium silt) and the lowest mean size was observed at station 64 (2.17Ø fine sand). For sorting, the sediments are poorly sorted with an average value of 1.14Ø (poorly sorted) which ranged from 0.49-1.82Ø. The highest sorting is observed at station 5 (1.82Ø poorly sorted) and the lowest sorting is observed at station 11 (0.49Ø, well sorted). Skewness, on the other hand, indicates whether the sediment is in excess of fine or coarse fraction. Positive values indicate that the normal size

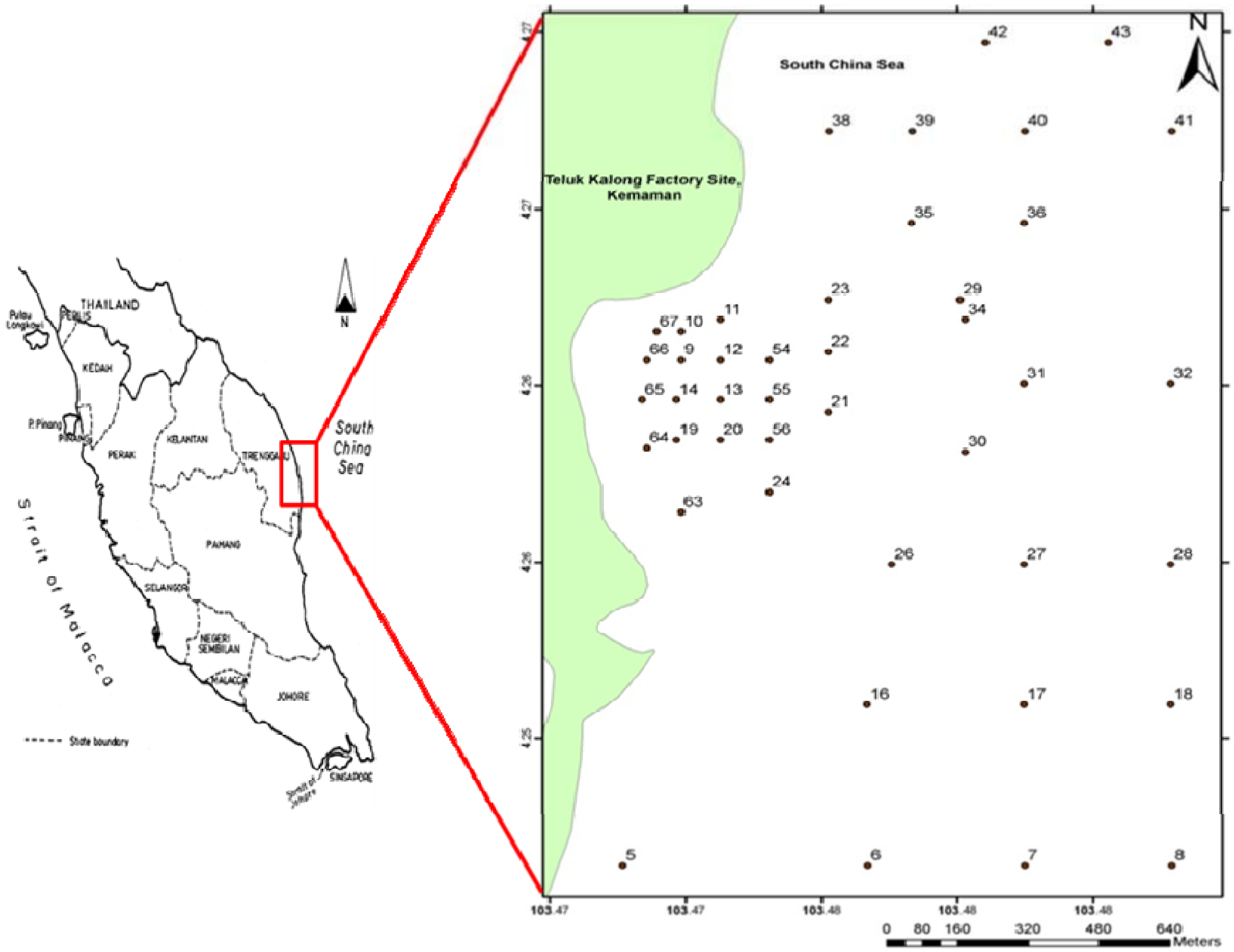


**Fig. 1 Location of sampling stations in the study area.**

**Table 2 Grain size in the sediments of the study area.**

| Station | Mean (Ø) | Sorting | Skewness |
|---|---|---|---|
| 5 | 5.495 | 1.817 | 0.696 |
| 6 | 4.543 | 1.778 | 1.021 |
| 7 | 4.442 | 1.589 | 1.342 |
| 8 | 4.194 | 1.606 | 1.193 |
| 9 | 3.184 | 0.989 | 2.529 |
| 10 | 3.021 | 0.704 | 1.735 |
| 11 | 2.830 | 0.492 | -0.030 |
| 12 | 3.044 | 0.700 | 1.960 |
| 13 | 3.176 | 0.808 | 2.838 |
| 14 | 2.994 | 0.686 | 1.388 |
| 16 | 3.785 | 1.348 | 2.044 |
| 17 | 4.119 | 1.496 | 1.649 |
| 18 | 4.024 | 1.536 | 1.248 |
| 19 | 3.051 | 0.729 | 1.572 |
| 20 | 3.201 | 0.546 | 0.005 |
| 21 | 3.350 | 1.318 | 0.896 |
| 22 | 3.273 | 1.265 | 1.574 |
| 23 | 3.186 | 0.913 | 2.931 |
| 24 | 3.406 | 1.114 | 2.471 |
| 26 | 3.556 | 1.043 | 2.505 |
| 27 | 4.164 | 1.481 | 1.696 |
| 28 | 3.968 | 1.486 | 1.535 |
| 29 | 4.010 | 1.431 | 1.863 |
| 30 | 3.901 | 1.377 | 1.959 |
| 31 | 4.104 | 1.504 | 1.676 |
| 32 | 3.857 | 1.574 | 1.083 |
| 34 | 3.277 | 1.152 | 1.955 |
| 35 | 3.415 | 1.530 | 1.153 |
| 36 | 3.947 | 1.448 | 1.828 |
| 38 | 3.063 | 0.552 | 0.046 |
| 39 | 3.179 | 1.153 | 2.383 |
| 40 | 3.887 | 1.399 | 1.912 |
| 41 | 3.911 | 1.441 | 1.816 |
| 42 | 3.274 | 1.117 | 0.682 |
| 43 | 3.638 | 1.257 | 2.258 |
| 54 | 3.095 | 1.053 | 0.435 |
| 55 | 3.358 | 1.115 | 2.563 |
| 56 | 3.359 | 1.030 | 2.563 |
| 63 | 2.627 | 0.559 | -0.057 |
| 64 | 2.176 | 0.809 | -0.346 |
| 65 | 2.349 | 0.672 | -0.388 |
| 66 | 2.333 | 0.828 | -0.923 |
| 67 | 2.741 | 0.555 | -0.063 |
| Average | 3.50 | 1.44 | 1.35 |

distributions are influenced by fine sediment while the negative values indicate coarse sediment sizes. In this study, the sediments are very positively skewed with average value of 1.37Ø (very positively skewed) which ranged from 2.93Ø to 0.39Ø. The highest skewness is recorded at station 9 (2.53Ø, very positively skewed) and the lowest skewness is recorded at station 66 (0.923Ø, very negatively skewed).

*4.1 Spatial Distribution Patterns of Grain Size in the Study Area*

The distribution patterns of grain size are shown in Figs. 2-4. Mean size of the sediments (Fig. 2) increased with the distance from the shores and a corresponding rise in the percentage of silt and clay which is high at the port entrance. Currents distribute sand and larger particles along the coasts while wave action carries the silts and clay to deeper waters [6]. For sorting, results show that the sediments are characterized as poorly sorted to moderately sorted (Fig. 3). Poor sorting is a result of an environment formed where energy fluctuates over a wide spectrum [6]. The distribution patterns of sorting are more or less the same with the sediment mean size distribution (Fig. 2).

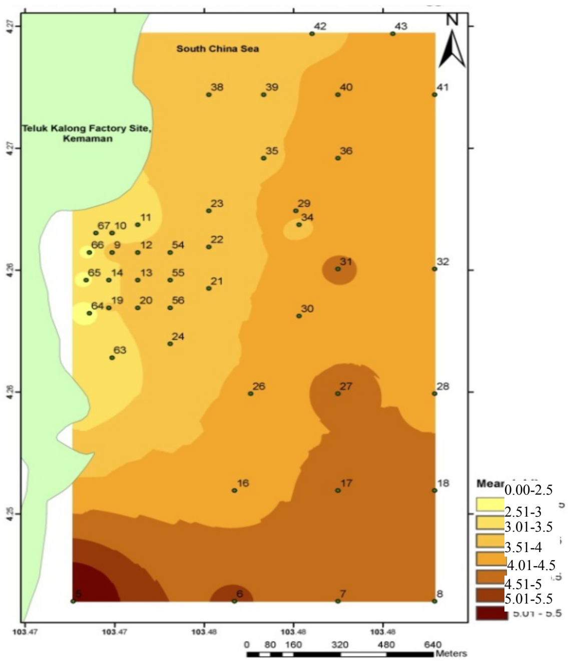


**Fig. 2 Distribution patterns of mean size.**

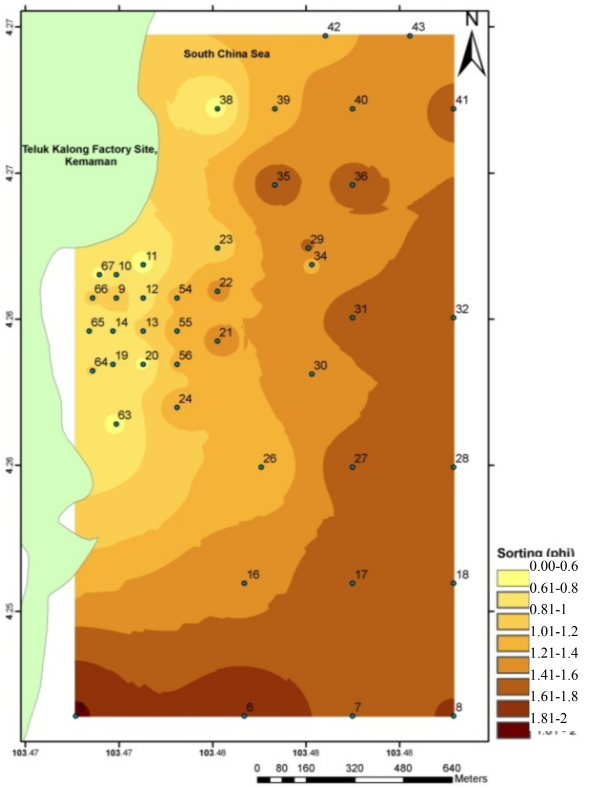


**Fig. 3 Distribution patterns of sorting.**

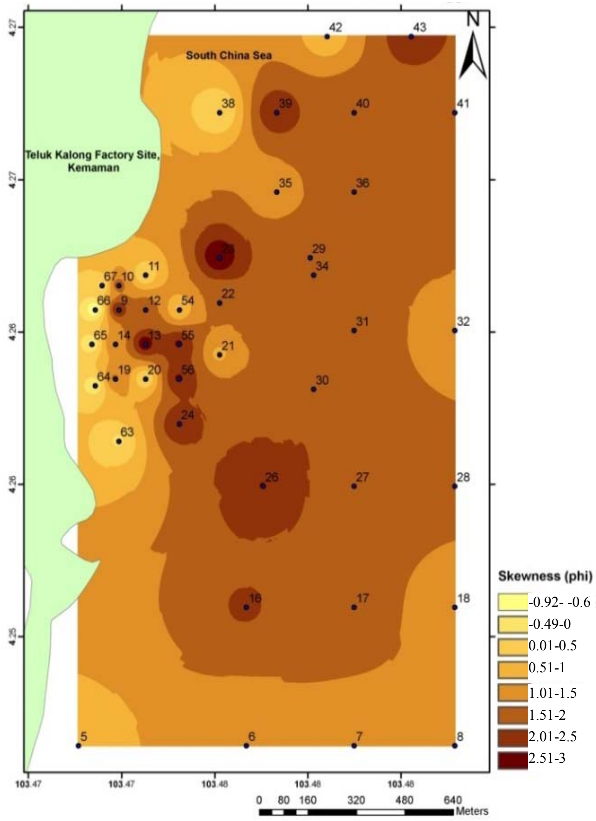


**Fig. 4 Distribution patterns of skewness.**

Skewness, however, has shown different distribution patterns. Most probably, during sampling period the sediments have been transported by turbidity currents and the constant presence of other types of energy that occasionally regulate the sediment transport and sedimentation. The positive skewness indicates the peak of the grain size distribution towards the fine-grained sizes which is a result of shallow currents and wave action prevailing in the area. Negative skewness might be due to the effects of wave actions which transport smaller particles towards offshore leaving coarser ones closer to the coastline (Fig. 4). Results on the texture analysis show that the study area is dominated with sandy texture (60.5%) followed by loamy sand (20.9%), sandy clay (16.3%) and silty loam (2.3%) (Fig. 5). The results on texture reflect to the results on mean size which shows coarse sediments that is dominant.

### *4.2 Spatial Distribution Patterns of the Trace Metallic Elements in the Study Area*

Table 3 shows the concentrations of metallic trace elements in the study area and the distribution patterns are shown in Figs. 6-11. Cu and Zn are almost similar (Figs. 6 and 7). The higher concentrations are detected at the port entrance (stations 6, 7) and offshore stations (station 32) compared to mid and near shore stations. There are also stations at the upper shore beach discharge and marine outfall which are higher in concentrations. The increase in contents of these trace metals might be due to anthropogenic inputs, industrialization near

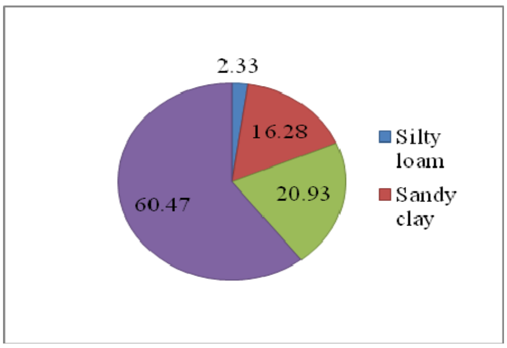


**Fig. 5 Sediment texture in the study area.**

**Table 3 Concentrations of metallic trace elements (μg/g dry wt.) in sediments of the study area.**

| Station | Cr | Ni | Cu | Zn | Cd | Pb |
|---|---|---|---|---|---|---|
| 5 | 47.66 | 17.62 | 14.81 | 57.30 | 0.12 | 32.86 |
| 6 | 77.64 | 44.46 | 14.33 | 59.40 | 0.13 | 45.06 |
| 7 | 44.84 | 28.66 | 8.77 | 44.80 | 0.27 | 33.66 |
| 8 | 19.56 | 38.66 | 13.41 | 32.60 | 0.14 | 45.26 |
| 9 | 60.04 | 29.86 | 9.33 | 51.00 | 0.14 | 35.06 |
| 10 | 36.84 | 13.06 | 5.45 | 38.20 | 0.05 | 16.46 |
| 11 | 31.28 | 13.66 | 2.99 | 39.20 | 0.03 | 18.66 |
| 12 | 36.04 | 21.71 | 13.71 | 17.60 | 0.13 | 23.86 |
| 13 | 25.06 | 6.48 | 5.27 | 46.10 | 0.11 | 29.46 |
| 14 | 72.66 | 24.22 | 11.33 | 73.30 | 0.05 | 37.66 |
| 16 | 56.26 | 13.32 | 9.69 | 63.10 | 0.14 | 35.06 |
| 17 | 34.74 | 13.28 | 12.57 | 42.54 | 0.17 | 43.46 |
| 18 | 48.06 | 14.76 | 8.21 | 50.70 | 0.01 | 26.86 |
| 19 | 31.14 | 4.40 | 5.21 | 36.74 | 0.13 | 34.86 |
| 20 | 54.66 | 9.50 | 36.39 | 67.70 | 0.10 | 29.26 |
| 21 | 44.66 | 9.50 | 9.61 | 49.70 | 0.12 | 35.86 |
| 22 | 49.06 | 10.94 | 7.05 | 55.70 | 0.09 | 27.66 |
| 23 | 14.96 | 9.86 | 7.37 | 27.22 | 0.05 | 28.06 |
| 24 | 28.14 | 7.72 | 32.79 | 41.14 | 0.17 | 36.06 |
| 26 | 48.46 | 9.82 | 6.73 | 58.70 | 0.11 | 24.26 |
| 27 | 43.26 | 12.80 | 8.45 | 54.30 | 0.08 | 31.46 |
| 28 | 29.74 | 10.38 | 7.95 | 36.34 | 0.15 | 34.46 |
| 29 | 46.26 | 13.50 | 8.97 | 54.10 | 0.07 | 35.26 |
| 30 | 39.06 | 13.06 | 10.23 | 52.70 | 0.13 | 34.06 |
| 31 | 31.54 | 10.32 | 8.95 | 51.74 | 0.12 | 36.86 |
| 32 | 38.46 | 12.50 | 41.39 | 49.50 | 0.23 | 37.46 |
| 34 | 35.34 | 10.62 | 8.73 | 43.54 | 0.19 | 39.26 |
| 35 | 26.66 | 6.74 | 5.81 | 40.10 | 0.13 | 26.26 |
| 36 | 37.66 | 10.24 | 6.39 | 42.30 | 0.04 | 27.26 |
| 38 | 33.86 | 3.54 | 4.49 | 36.70 | 0.05 | 16.26 |
| 39 | 39.66 | 8.88 | 6.07 | 37.50 | 0.09 | 23.46 |
| 40 | 11.46 | 2.58 | 9.63 | 24.30 | 0.09 | 24.06 |
| 41 | 32.26 | 9.74 | 5.93 | 25.70 | 0.05 | 21.46 |
| 42 | 28.46 | 6.88 | 5.51 | 42.10 | 0.14 | 27.66 |
| 43 | 17.76 | 5.12 | 5.25 | 30.02 | 0.05 | 25.46 |
| 54 | 21.46 | 3.52 | 2.99 | 31.70 | 0.10 | 20.06 |
| 55 | 32.66 | 4.88 | 6.09 | 35.79 | 0.25 | 30.26 |
| 56 | 22.26 | 4.12 | 6.75 | 19.90 | 0.08 | 24.86 |
| 63 | 11.78 | 2.32 | 2.31 | 17.62 | 0.20 | 8.74 |
| 64 | 10.22 | 1.74 | 1.95 | 26.72 | 0.22 | 33.06 |
| 65 | 8.46 | 0.78 | 2.75 | 25.79 | 0.18 | 20.46 |
| 66 | 8.30 | 1.98 | 2.63 | 24.70 | 0.06 | 21.26 |
| 67 | 21.46 | 1.90 | 4.43 | 26.50 | 0.04 | 22.26 |

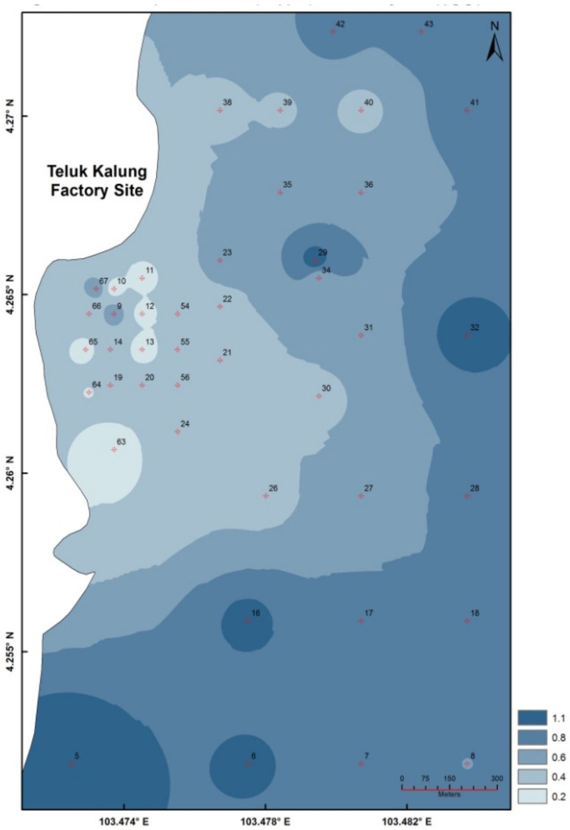


**Fig. 6 Distribution patterns of Cu.**

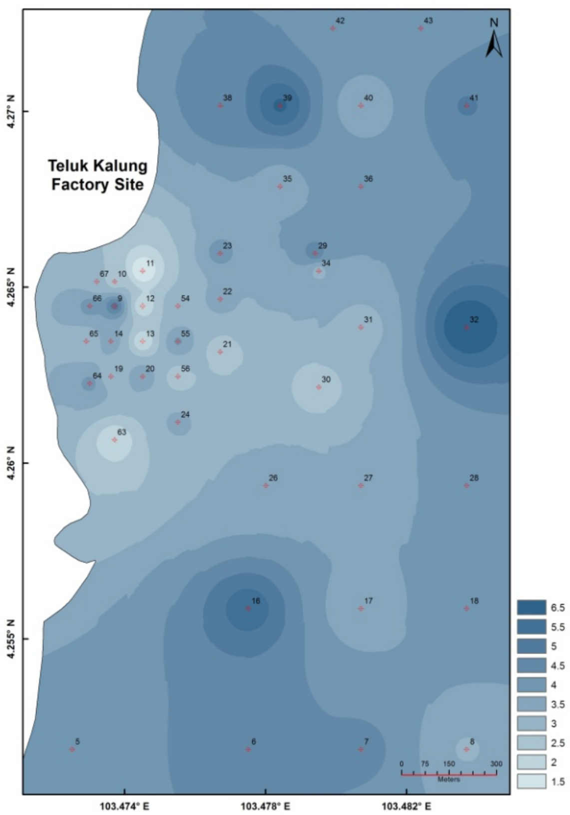


**Fig. 7 Distribution patterns of Zn.**

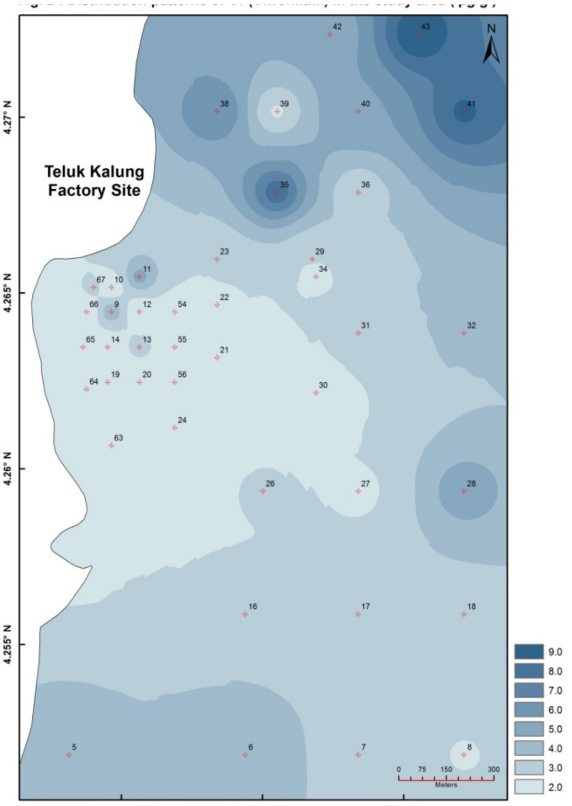


Fig. 8 Distribution patterns of Cr.

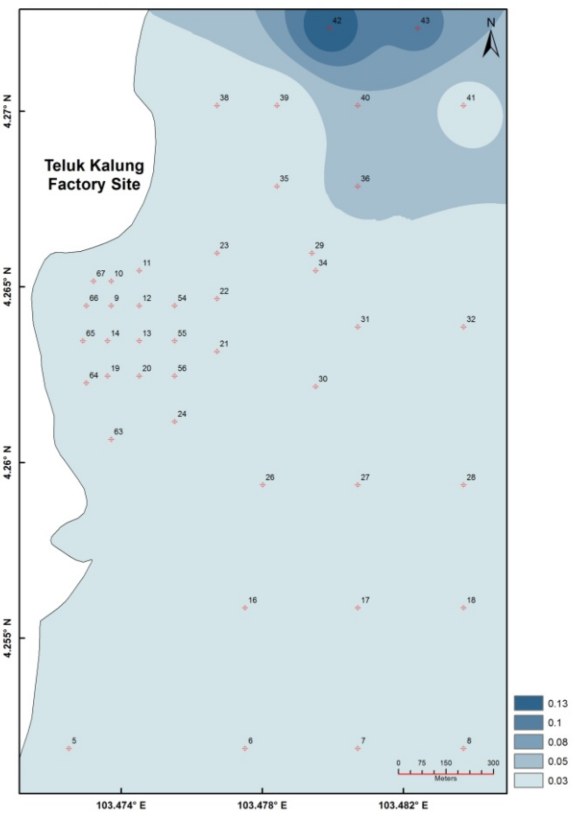


Fig. 9 Distribution patterns of Cd.

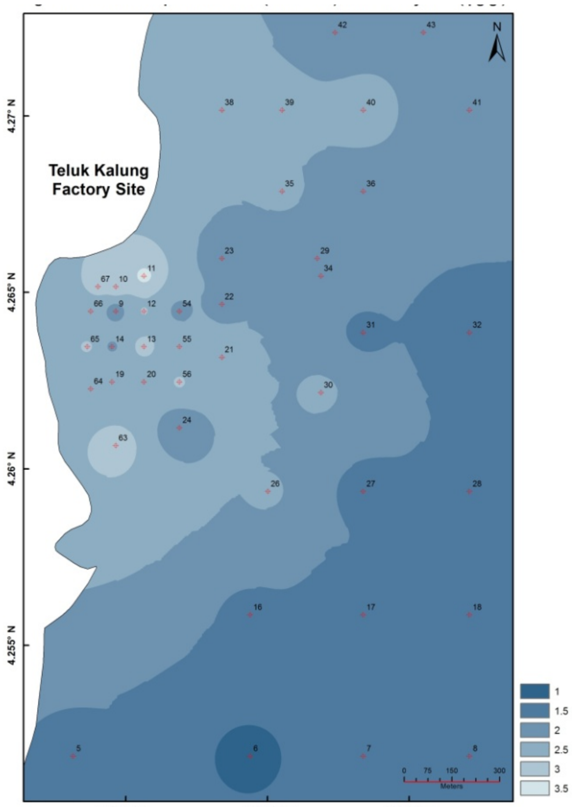


Fig. 10 Distribution patterns of Pb.

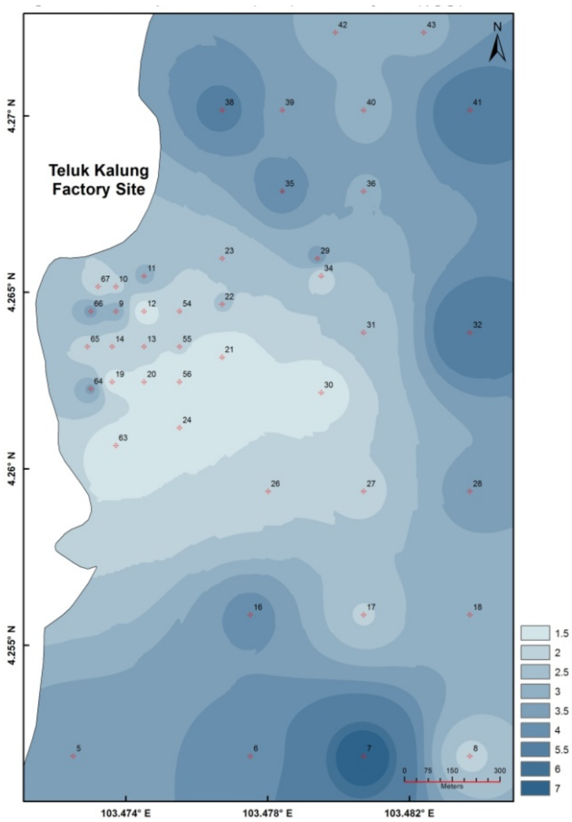


Fig. 11 Distribution patterns of Ni.

the area, the texture and mineralogy of the sediments. For Cr (Fig. 8), higher concentration was observed at the uppermost portion of the factory site and at the port entrance which reflects to the sediment texture ranging from sand to silt loam (Fig. 5). Dramatically, Cd (Fig. 9) distribution shows higher concentration in only two stations (stations 42-43) which are at the uppermost portion of the study area while the rest shows a uniform distribution. This might be due to anthropogenic inputs form industrialization, agricultural activities nearby surrounding area, being of terrigenous origin. Pb (Fig. 10) distribution shows higher at the port entrance and from the offshore stations in a decreasing manner towards mid and nearshore stations.

Ni (Fig. 11), on the other hand, showed higher concentrations in almost the whole study area except at some stations located at the marine outfalls. This might be attributed to its being of terrigenous origin.

Pollution assessment was done to determine whether there are anthropogenic inputs in the study area. Results show that enrichment of metallic trace elements studied ranked in the following order according to the contamination category [7]: Pb > Cd > Zn > Mn > Fe > Cu > Ni > Cr with average EF value of 5.32, 3.84, 2.32, 2.22, 1.94, 1.86, 1.75 and 0.76, respectively. Pb is significantly enriched. Cd, Zn and Mn are moderately enriched while Cr, Cu, Fe and Ni are in the category of deficiency to minimal enrichment. This proves that there are anthropogenic sources from adjacent industrial area. When EF > 5, a significant portion of a given metal is delivered from non-crustal materials, or non-natural weathering processes, and then anthropogenic sources become an important contributor. This might be due to the use of the leaded petrol and heavy shipping traffic at surrounding area which can increase its concentration in the marine sediment. In marine sediments from the coastal environment of Peninsular Malaysia, concentrations of Pb indicate some enrichment above the natural global value (in shale) in the coast of Kemaman [8].

## 5. Conclusions

Based on the findings, it can be concluded that coarse sediments had lower levels of metallic trace elements while finer sediments had higher levels. In addition, the sediments in the study area are significantly polluted with Pb, moderately polluted with Cd and Zn which might be due to waste discharges from industries and heavy shipping activities in the surrounding area.

## References


[1] R. Guevara, A. Rizzo, R. Sanchez, Heavy metal inputs in northern Patagonia lakes from short sediment core analysis, J. Radioanal Nucl Chem. 265 (3) (2005) 481-493.

[2] D. Baldantoni, A. Alfani, P. Di Tommasi, G. Bartoli, A. Virzo De Santo, Assessment of macro and microelement accumulation capability of two aquatic plants, Environ. Pollut. 130 (2004) 149-156.

[3] Z.L. Chen, S.Y. Xu, L. Liu, J. Yu, L.Z. Yu, Spatial distribution and accumulation of heavy metals in tidal flat sediments of Shanghai coastal zone, Acta Geographica Sinica 55 (6) (2004) 641-651.

[4] B.Y. Kamaruzzaman, Geochemistry of the marine sediment: Its paleoceanographic significance, Ph.D. Dissertation, Hokkaido University, Japan, 1999.

[5] H.K. Wedepohl, The composition of the continental crust, Geochimica et Cosmochimica Acta 59 (7) (1995) 1217-1232.

[6] T. Garrison, Essentials of Oceanography, Wadsworth Publisphing Co., Belmont, California, 1995, pp. 80-81.

[7] R.A. Sutherland, Bed sediment-associated trace metals in an urban stream, Oahu, Hawaii, Environmental Geology 39 (2000) 611-627.

[8] A.S. Ahmad, Distribution of some heavy metals in the Kemaman coast, Terengganu, M.Sc. Thesis, Universiti Pertanian Malaysia, Malaysia, 1996.

Journal of Earth Science and Engineering 4 (2014) 88-93

# Presentation of the Module “GRAPHS” for Analyzing Geobotanical Data

Alexander Novakovskiy

*Laboratory of Computer Technology and Modeling, Institute of Biology, Komi Science Center, Russian Academy of Science, Syktyvkar 167982, Russia*

Received: January 05, 2014 / Accepted: February 08, 2014 / Published: February 25, 2014.

**Abstract:** This paper describes the program module “GRAPHS” which was developed for data processing in geobotany and ecology fields. The “GRAPHS” has a simple interface and is integrated into the Microsoft Excel. This allows users to use all features of Microsoft Excel for storage and preparation data for analysis. Calculation of the most common similarity indexes (Jaccarda, Sorenson, Ohai etc.) and their visualization by using different algorithms of the graph theory or hierarchical cluster analysis allows simplifying and accelerating the process of data analysis in ecology or geobotany and makes it clearer. Also, three ordination methods—PCA (principal components analysis), CA (correspondence analysis), NMS (nonmetric multidimensional scaling)—were implemented in the module. The module can be used for vegetation classification, and be used to allocate diagnostic species or to search environmental factors most strongly impact on vegetation. Algorithms of data analysis which were implemented in the module “GRAPHS” have universal nature so they can be applied in many other fields of science.

**Key words:** Geobotany, ecology, cluster analysis, ordination, graphs theory, Microsoft Excel.

## 1. Introduction

In present days, there are many computer programs developed for statistical analysis and data visualization ranging from large, complicated and expensive packages, such as STATISTICA and SPSS (statistical package for the social sciences), to relatively small and inexpensive packages such as PC-ORD [1] and Canoco [2]. In addition, there are some freeware statistical programs. The “R” package is one of the most well known freeware statistical programs [3]. Often, researchers (especially in the ecology and biology fields) have difficulties using these kinds of software including: (1) preparing data for analysis (programs often use special data formats not compatible between each other); (2) interpreting results of statistical analysis; and (3) using program with unusual or unclear interfaces. It is very helpful to have some tools to make statistical analysis as easy as possible without a lot of efforts.

**Corresponding author:** Alexander Novakovskiy, Ph.D., research fields: geobotany, ecology and statistical analysis. E-mail: novakovsky@ib.komisc.ru.

## 2. The Module Description

We have designed the “GRAPHS” to help scientists in statistical data proceedings. This module is an Excel add-on. After its installation new submenu appears in Excel (Fig. 1). Full compatibility allows using all the standard Excel functions to convert data or to prepare them for analysis.

The data source for this sub-module is a classical geobotanical table where rows are releves (objects) and columns are species (their properties) or other

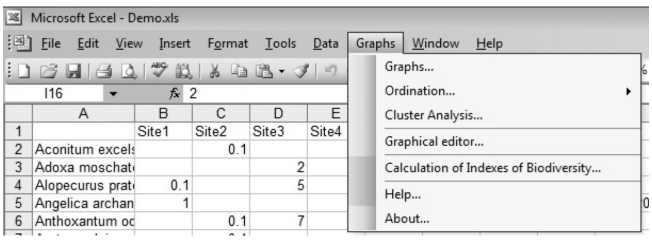


**Fig. 1 The Excel submenu—“GRAPHS”.**

ecological parameters. For the users' convenience, ranges that contain data can be defined automatically. However, to avoid errors in determining ranges, it is better to follow some simple rules including: (1) only one (first) row should contain information about objects captions; (2) only one (first) column should hold properties names; and (3) only numeric values should be presented in all other cells.

The "GRAPHS" menu provides three groups of methods for analysis:

(1) Cluster Analysis. There are two groups of options in the dialog window for cluster analysis. The first option—similarity indexes used to make the table of distances between the objects. In the module, some of the most common similarity indexes used in botany were developed (Appendix A) [4-7]. The second option is the method of objects grouping. Three methods are developed by the moment: the nearest neighbor method, UPGMA (unweighted pair group method with arithmetic mean) and Ward's method of clustering (Fig. 2a) [8] (Appendix B).

(2) Ordination. In the "GRAPHS" module three ordination methods are implemented: PCA, CA and NMS (Fig. 2b). There is a lot of literature devoted to the subject of ordinations [1, 9-11] (Appendix C).

(3) Graph Theory. Like in the cluster analysis, a user selects a similarity index to calculate the matrix of distances between the objects and a form of presenting this matrix. The following forms of presentation are implemented: (a) circle form (all objects are located in a circle) and thickness of lines shows the value of similarity—the higher coefficient of similarity of the thicker line; (b) weighted tree (only the highest similarities are shown); (c) star form; and (d) splitting graph into connected components (Fig. 3) [12] (Appendix D). The graph theory allows presenting fewer objects than the other methods, specifically no more than 30-40 objects. However, specialists can easily interpret this form of graphical representation of data.

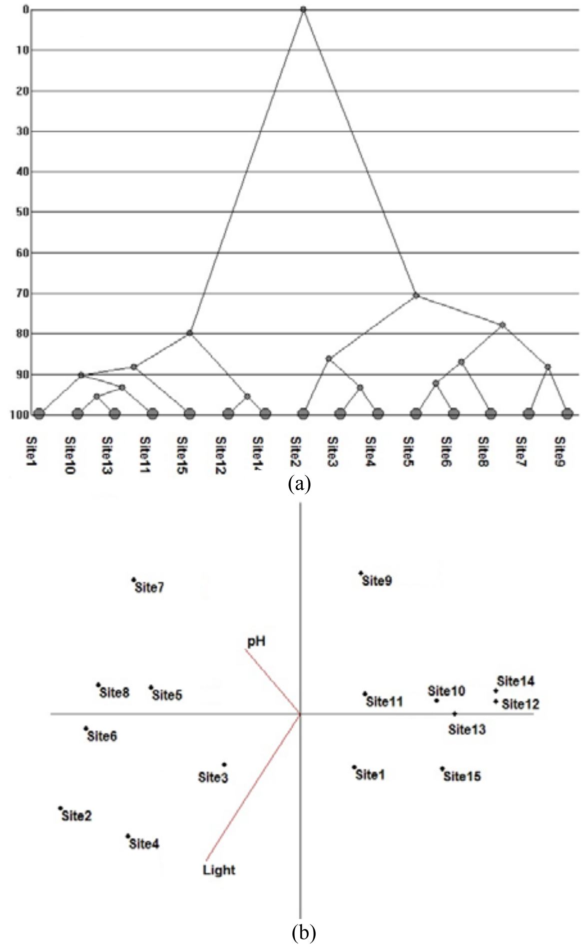


**Fig. 2 An example of the resulting figures output from "GRAPHS." (a) Cluster analysis (Ward clustering) and (b) ordination (NMS method).**

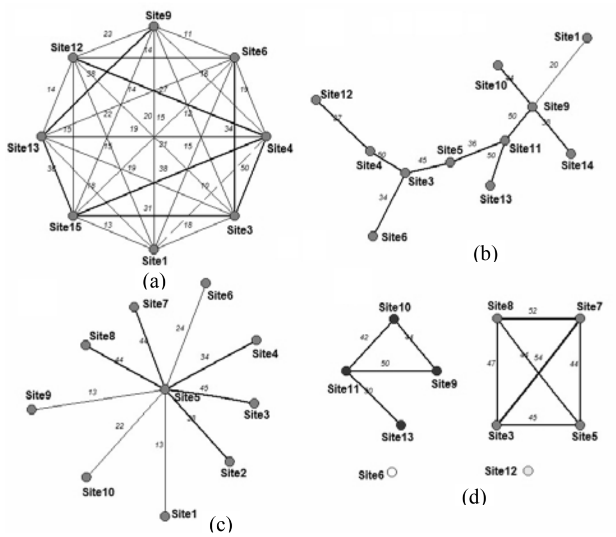


**Fig. 3 Different forms of graph theory presentation output from the "GRAPHS." (a) Circle graph; (b) tree graphs (connected graph without cycles); (c) star graph; and (d) connected components.**

## 3. Conclusions

The “GRAPHS” module speeds up the process of data analysis and makes it more intuitive. It was achieved by automatization of calculations of different similarity indexes and by the data visualization using graph theory, ordination and cluster analysis. Close connection with Microsoft Excel allows using any widespread data format as a data source.

Combination of different approaches of the analysis provides correct data processing avoiding disadvantages that are inherent to individual methods.

Methods implemented in the module are universal, so the module “GRAPHS” can be used in various fields of science.

For more information about the “GRAPHS”, you can download demo version and visit the website http://m-graphs.com/index.php/en.

## References

[1] R.H.G. Jongman, C.J.F. Ter Braak, O.F.R. Van Tongeren, Data Analysis in Community and Landscape Ecology, Pudoc, Wageningen, Netherlands, 1987.

[2] J. Leps, P. Smilauer, Multivariate Analysis of Ecological Data Using CANOCO, Cambridge University Press, NewYork, 2003.

[3] K. Seefeld, E. Linder, Statistics Using R with Biological Examples, Department of Mathematics & Statistics, University of New Hampshire, Durham, NH, USA, 2007.

[4] L. Legendre, P. Legendre, Numerical Ecology, 2nd ed., Elsevier Science BV, Amsterdam, Netherlands, 1998.

[5] D. Mueller-Dombois, H. Ellenberg, Aims and Methods of Vegetation Ecology, Blackburn Press, NY, USA, 2003.

[6] J.P. Guilford, Tatistics in Psychology and Education, McGraw-Hill, New York, 1942.

[7] V.I. Vasilevich, Statistical Methods in Geobotany, Nauka, Leningrad, Russia, 1969.

[8] J.H. Ward, Hierarchical grouping to optimize an objective function, Journal of the American Statistical Association 301 (1963) 236-244.

[9] B. McCune, J.B. Grace, D.L. Urban, Analysis of Ecological Communities, MjM Software Design, Oregon, USA, 2002.

[10] C.J.F. Ter Braak, Canonical correspondence analysis: A new eigenvector technique for multivariate direct gradient analysis, Ecology 67 (1986) 1167-1179.

[11] I.C. Prentice, Non-metric ordination methods in ecology, Journal of Ecology 65 (1977) 85-94.

[12] J.A. Bondy, U.S.R. Murty, Graph Theory with Applications, Elsevier Science, NY, USA, 1982.

[13] W.S. Torgerson, Multidimensional scaling: Theory and method, Psychometrica 17 (1952) 401-419.

**Appendix**

**Appendix A**: **Similarity Indexes.**

1. Binary indexes

Binary similarity indexes are based on summarized 2 × 2 frequency table of presence or absence:

| | | Object 2 | | |
|---|---|---|---|---|
| | | + | - | |
| Object 1 | + | *a* | *b* | (a + b) |
| | - | *c* | *d* | (c + d) |
| | | (*a* + *c*) | (b - *d*) | *N* |

where, *a* is the number of presence of properties in both objects (for example, joint meetings species in both releves), *d* is the number of absence of the properties (the number of missing species in both releves), *b* and *c* are the numbers of presence of properties only in Objects 1 and 2, respectively (the number of species only in releve 1 or 2), *N* is the total number of properties (the total number of species).

The following binary indexes were implemented in GRAPHS:

$$\text{Jaccard—} K_j = \frac{a}{a+b+c} \times 100 \tag{1}$$

$$\text{Sorensen—} K_s = \frac{2a}{(a+b)+(a+c)} \times 100 \tag{2}$$

Ohiai— $$K_o = \frac{a}{\sqrt{(a+b)(a+c)}} \times 100 \quad (3)$$

Brave— $$r = \frac{ad-bc}{\sqrt{(a+b)(a+c)(b+d)(c+d)}} \times 100 \quad (4)$$

2. Quantitative indexes

Quantitative indexes are realized in GRAPHS:

Quantitative Sorensen (Steinhaus)— $$K_s = \frac{2 \times \sum_{i=1}^{N} \min(A_i, B_i)}{\sum_{i=1}^{N} A_i + \sum_{i=1}^{N} B_i} \times 100$$

Indexes of inclusion— $$K_{AB} = \frac{\sum_{i=1}^{N} \min(A_i, B_i)}{\sum_{i=1}^{N} A_i} \times 100, \quad K_{BA} = \frac{\sum_{i=1}^{N} \min(A_i, B_i)}{\sum_{i=1}^{N} B_i} \times 100$$

where, $A_i$ and $B_i$—quantitative characteristics.

The Pearson correlation and the Kendall rank correlation are also used in module.

## Appendix B: Cluster Analysis (Agglomerative Clustering).

Agglomerative clustering builds a hierarchy from individual elements by progressively merging clusters. The algorithm is composed of the following steps:

(1) Calculate a similarity matrix using indexes (Appendix A);

(2) Mark all the elements as separate clusters;

(3) Find two closest clusters. Similarities between clusters are calculated in different ways:

(a) Nearest neighbor clustering— $d = \min\{d(x, y) : x \in A, y \in B\}$

(b) Unweighted pair group with arithmetic mean (UPGMA)— $d = \frac{1}{|A| \times |B|} \sum_{x \in A} \sum_{y \in B} d(x, y)$

(c) Ward’s method— $d = \|x - y\|^2, x \in A, y \in B$. (For Ward’s method only Euclidian distance is used)

where $d$—similarity between clusters $A$ and $B$, $d(x, y)$—similarity between elements from similarity matrix.

(4) Mark these two elements as belonging to one cluster;

(5) If all objects are in one cluster, stop. Else, go to step “3”.

Ward’s method uses Euclidian distances instead of similarity indexes, so we need to convert them: $d' = \frac{dMax - d}{dMax} \times 100$, where $dMax$ is maximum distance between clusters, $d$ is current distance. Thus, the maximum distance is 0, zero distance is 100%.

## Appendix C: Ordination.

3. PCA—Principal component analysis

Step 1: Centering the data matrix X by columns

$c_{i,j} = a_{i,j} - (\frac{1}{n} \sum_{i=1}^{n} a_{i,j})$, where $a_{i,j}$—elements of data matrix.

Step 2: Normalization of the centered data

$x_{i,j} = \frac{c_{i,j}}{\sigma_j}$ or $x_{i,j} = \frac{c_{i,j}}{s_j}$ (dependence from settings)

Step 3: Calculation of cross-products matrix Σ

$$\Sigma = \frac{1}{n}[X'X] \quad (C_1)$$

Step 4: Find eigenvalues and eigenvectors of this matrix Σ. It is a real symmetric matrix, so we use QL/QR algorithm to find eigenvalues and eigenvectors. Rank the eigenvalues descending.

Step 5: Usually we use only two largest eigenvalues and corresponding eigenvectors to make axis of a PCA diagram.

Step 6: Find "scores" for each case (or object) on first two axes. Scores are the original matrix multiplied by the matrix of eigenvectors.

4. NMS—Nonmetric multidimensinal scaling

Step 1: Definition of starting configuration. It can be produced with a random number generator or using another ordination algorithm (PCA for instance). By default, we use the Torgerson algorithm [13].

Step 2: Normalize configuration $x_{ij} = \frac{x_{ij} - \bar{x}_l}{\sqrt{\sum_{j=1}^{r}\sum_{i=1}^{n}(x_{ij} - \bar{x}_j)^2 / (n \cdot r)}}$

where $\bar{x}_j$—the average value of the column.

Step 3: Calculate matrix $D$ of the Euclidian distance between elements: $d_{ab} = \sqrt{\sum_{i=1}^{r}(x_{ai} - x_{bi})^2}$

Step 4: Correspond the $n*(n-1)/2$ elements of the original matrix to the distance matrix $D$. Rank elements of the original matrix and put elements of $D$ in the same order.

Step 5: Make matrix $\hat{D}$ that consists of elements $D$ in monotonic order.

Step 6: Calculate stress function:

$$S_1 = \sqrt{\frac{\sum_{i<j}(d_{ij} - \hat{d}_{ij})^2}{\sum_{i<j} d_{ij}^2}}$$ —stress function (Kruskal 1)

$$S_2 = \sqrt{\frac{\sum_{i<j}(d_{ij} - \hat{d}_{ij})^2}{\sum_{i<j}(d_{ij} - \bar{d})^2}}$$, where $\bar{d} = \frac{2}{n(n-1)}\sum d_{ij}$ (Kruskal 2)

If elements of the matrix $D$ is monotonic $S_1$ ($S_2$) = 0.

Step 7: If $S_1$ ($S_2$) is less than threshold that was set by user before *stop* the algorithm.

Step 8: Find new configuration using gradient descent. Go to step 2.

5. CA—Correspondence analysis

Step 1: Calculate the matrix grand total ($n = \sum_i \sum_j a_{ij}$) and weighting coefficients for rows ($v_i = \sum_j a_{ij} / n$) and columns ($w_j = \sum_i a_{ij} / n$). $a_{ij}$ is the elements of the data matrix $A$.

Step 2: Calculate the matrix of standardized residuals $B$. $b_{ij} = (a_{ij} / n - v_i w_j) / \sqrt{v_i w_j}$

Step 3: Calculate cross-products matrix for objects $S = B'B$.

Step 4: $S$ is the symmetric matrix, so it is used QL/QR algorithm to find eigenvalues $\{\lambda\}$ and eigenvectors.

Step 5: Rank eigenvalues descending and select first $k$ largest values and $k$ corresponding eigenvectors. $k$ is the number of axis (usually $k = 2$).

Step 6: Calculate object’s coordinates by multiplying each element of eigenvectors to scaling factor ($SF$). $SF = \max\{\lambda\} / v_i$.

Step 7: Repeat steps 3-6 for cross-products matrix of properties $S_1 = BB'$ and calculate properties coordinates.

**Appendix D**: **Using the Graphs Theory.**

(1) Calculate the similarity matrix between elements (Appendix A).

(2) Make a graph where nodes are elements and edges represent coefficients from similarity matrix.

(3) Choice form of the graph representation:

(a) Circle graph is complete graph—$K_n$, where $n$—number of elements. All edges are shown.

(b) Tree graph is an undirected connected graph without cycles. Edges with largest coefficients are selected.

(c) Star graph is a tree graph with one internal node and $n$-1 leaves. All edges connected with internal node are shown.

(d) Connected components are set of subgraphs, each of them is a connected graph (any two nodes are connected to each other by path). Edges with coefficients large than threshold value are displayed.

Journal of Earth Science and Engineering 4 (2014) 94-100

# Unknown Signs and Symbols on Egyptian Prehistoric Naqada Stone Palettes

Valdis Seglins

*Faculty of Geography and Earth Sciences, University of Latvia, Riga LV-1010, Latvia*

Received: January 06, 2014 / Accepted: January 25, 2014 / Published: February 25, 2014.

**Abstract:** Although stone palettes from the Naqada culture are well known, research has been focused mostly on those palettes which are richly decorated. However, streaks and fragments of individual signs are also often found on simple palettes of various shapes. This study shows that the majority of these palettes have quite a number of marks and sign fragments that have been made by different techniques and over a long period of time. This particularly applies to rhomboidal palettes, for most of which there are no ground to infer that they have been used for ritual purposes or for mixing beauty care compositions. It is more likely that they denote an early form of the visual symbol in later periods represented by the head of Ptah's staff.

**Key words:** Prehistoric Egypt, stone palettes, invisible signs and symbols, Ptah's staff.

## 1. Introduction

Stone palettes from the Badarian and Naqadian culture periods are well known already for over a century and many of them are excellent art masterpieces of that time. They served as ritual and utilitarian objects, i.e., as bases for placing offerings and preparation of beauty care compositions. These palettes were relatively well explored in the early 20th century thanks to the systematic research of Brunton and Caton-Thompson (1928) [1] and particularly of Petrie [2] carried out at the tombs discovered in the vicinity of Memphis as well as the sustained subsequent research work on these findings. Later research mostly covered individual palettes or their parts studied in greater detail in museums, mainly deciphering a few richly illustrated palettes that have been used in rituals. A more comprehensive summary of this research is still under way. There are several reasons for such delay, the most important of which are the relatively small number of palettes concentrated in museums (compared to little-known private collections) and also rather modest decoration or its absence on most of these palettes, thus limiting the possibilities of using them as sources of information about prehistoric Ancient Egypt. Nevertheless, in our view, by improving research methods applied to these black schist (slate, siltstone or mudstone) palettes, it is possible to find a great deal of useful information that has so far not been recognised.

The majority of ancient palettes are not displayed in museum permanent exhibitions, and just some museums have described them in detail in their catalogues, giving a description of the key parameters, usually accompanied by a small overview image. High-quality images of the palettes are still rare. In scientific publications, these images are incomplete and of insufficient quality. Moreover, images of many palettes are not available for more detailed study.

In this situation, the UCL (University College London), Petrie Museum collection online Catalogue and Francesco Raffaele's website "Corpus of Egyptian

**Corresponding author:** Valdis Seglins, Dr., professor, research fields: geoarchaeology, ancient Egypt and near east studies. E-mail: valdis.seglins@lu.lv.

Late Predynastic Palettes” [3] are very useful. These websites present not only images and descriptions of palettes, but also comprehensive bibliographies of relevant scientific literature, where one can look for more detailed information in the area of ancient palette research. Quite a considerable number of palettes are constantly available on sale in online stores and on auction websites. The offer also includes palettes of quite unusual shapes. It is worthwhile to study these palettes even if all they have is just fragments of barely distinguishable images. Yet, these fragments are the only source for reconstructing the original images. To succeed in this, the methodology of analysis needs to be improved.

## 2. Materials and Methods

The study is based on the analysis and interpretation of published images of palettes from the Predynastic period of Ancient Egypt. To the extent possible, more than 120 high-quality images were selected and the originals were saved in a specially created database.

A more detailed examinations of palette images from publications of the British Museum, Petrie Museum and Ashmolean Museum reveal quite a substantial number of old figure fragments on the simple zoomorphic palettes. These fragments are better preserved in the peripheral areas of palettes, where they are easier to recognise. Such figure fragments can be recognised on virtually all palettes. For example, on the MIN Hartebeest Palette (CG 54334) exhibited in the Cairo Museum, the figure of an antelope is accentuated, while earlier and simpler figure fragments for unknown reasons have not received any attention. In like manner, the lines and snake figure are not mentioned in the Ibis palette (Bruxelles, MRAH E6186) descriptions. Instances like these direct our attention to the need for more detailed study of these figures.

An important analysis from the point of view of developing the methodology was that of the relatively low-quality figure on Khnum (the Ram-Headed Creator God) palette [4]. Even though some of the lines on this palette were known previously, it was believed that they are not recognisable. And yet, fragments of quite many signs can be distinguished here (Fig. 1).

In the conventional practice of detailed artefact studies [5], images are processed by the reflectance transformation imaging technique to generate a file that represents the variation in intensity when the surface is illuminated from different directions, allowing recognising defects and surface alterations. This method enables observers to have a “virtual torch” experience that facilitates interpretation to be carried out more adequately. Unfortunately, the images at our disposal did not allow for fully availing of the benefits provided by this technology, and the acquired “synthetic” pictures lost the quality, contrast and details necessary for interpretation. However, this method is very efficient if it is possible to take high-resolution, stereoscopic pictures.

**Fig. 1 Khnum palette from the Egyptian Museum (Cairo), with recognized major lines.**

Due to the quality of images available for this study, less sophisticated image processing methods had to be used. Images were initially processed with Adobe Photoshop CS5 software, first of all making them black and white, then increasing the grey scale amplitude and magnifying the images as far as the pixel resolution allows without distortion. Further image processing was done with the conventional remote sensing data processing software Erdas Imagine, which allows identification of indistinct lines and their clusters and fragments. After that, image processing was continued manually, checking the detected lines and structures, distinguishing those that have been determined for sure from those that are only probable. This procedure allows reducing subjective interpretations and highlighting surely recognisable elements. To reduce subjective elements, the manual operations were additionally performed in three different pictures brightness (30%-50%) and contrast (50%-100%) settings. In many cases, it was helpful to reduce the Midtone value (dark colours only). Such manual adjustment allows distinguishing more exactly casual and later surface treatment marks from preserved fragments of purposefully inscribed old signs (Fig. 2). This could be successfully accomplished with such palettes as the Turtle shaped palette (Fitzwilliam Museum, E.7.1911), Make-up palette (Hunterian Museum Archaeology collections, Glahm D.1912.5), Cosmetic palette from tomb 1436 (University College London, No. 4240), etc..

## 3. Results

Using the chosen methodology, it is relatively easy to study flat-shaped palettes, and the main problems are related to the elimination of subjective factors during the process of interpretation. However, it is much more difficult to implement this method in examining rhombic- or rhomboidal-shape stone palettes. Only a few of these palettes have known embossed figures, while most of them have figures, symbols and signs that have not been recognized yet. A well-known exception is the Hippopotamus Hunt palette (Fig. 3), on which an effaced fairly complete figure has been recognised [6].

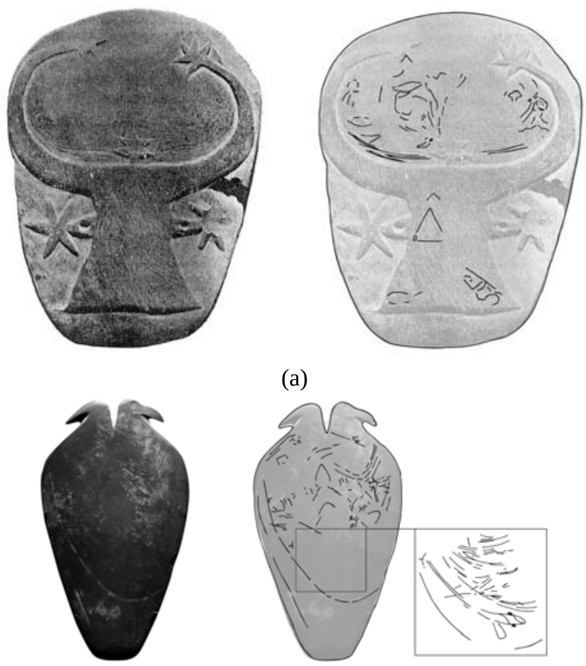

(a)

(b)

**Fig. 2 Manually engraved samples: (a) Gerzeh palette ("Hathor", cow-head palette; Egyptian Museum, Cairo, 34173); (b) double bird palette (Metropolitan Museum of Art, 22.4.4).**

**Fig. 3 Hippopotamus Hunt palette (Medelhavsmuséet, Stockholm E.M. 6000).**

However, the Hippopotamus Hunt palette is not the only one of the kind and, using the methodology described above, it is possible to detect fragments of various signs on many palettes of this shape. For example, such fragments are easily visible on the following palettes: the cosmetic palette from the Leeds Museum, the Fertility Goddess palette (Los Angeles County Museum of Art), the Rhomboid cosmetic palette from Ballas (Bolton Museum, 1896.44:09 and 1909.76:10), the Rhomboidal Palette (Museum of Fine Arts, Boston, 47.1641 and 03.1491), the Green schist cosmetic palette (collection of Joseph Klein, New York), several palettes at the Royal Museums for Art and History at Brussels and the great collection at the Petrie Museum, the University College, London.

The Rhomboidal Palette with Scorpion Relief (Tadashi Kikugawa's Collection) can be singled out as the most interesting one in this study, as there are fragments of many other signs recognisable next to the pronounced scorpion relief. Signs can be noticed all over the surface of the palette, and the most important ones are concentrated in the area just above the scorpion relief (Fig. 4).

Among the identified fragments of signs, a group of symbols are marked out that can be interpreted as the identification token of a ruler. This sign could be particularly studied by experts in the future, analysing a larger number of images of higher quality.

On the basis of the experience described above, a preliminary analysis of the rhomboidal palette from the collection of the LNMA (Latvian National Museum of Art) was also performed. Without in-depth examination of the surface of the palette, one can already recognise a curved stripe and a few isolated streaks that, upon closer scrutiny, are individual fragments of several signs (Fig. 5).

At the current stage of research, recognition of these elements is possible, leaving the interpretation for the next stage. On the surface of the palette, one can recognise signs that are quite different by their character and technical delivery, and the compositions have been made at different times, with long period in-between. This implies a long history of the use of this palette, possibly for different purposes, although making more substantiated conclusions would require an extensive comparative analysis.

## 4. Discussion

Rhomboidal palettes from Naqada culture are not uncommon. To gather data for this study, there were many dozens of these palettes identified just in European museums, although only a few of them are widely known. They differ significantly from other palettes by shape, and their meaning is unknown. Since the extensive research of Petrie [2], it is assumed that the uses of these palettes were quite traditional: for placing offerings, for mixing ingredients of beauty care preparations, and the like [7].

However, it is obvious that this shape is not handy for such functions, and the study detected the traces of such activities only on some of the palettes of this shape.

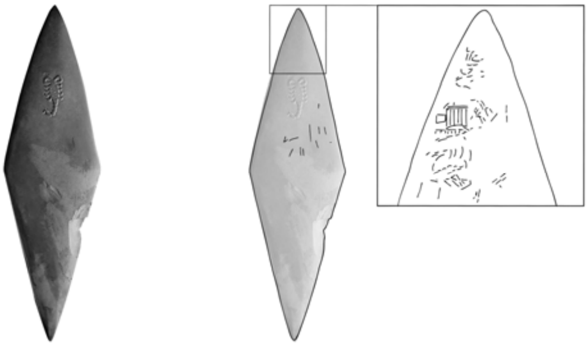

**Fig. 4 Fragments of unknown signs on the Rhomboidal Palette with Scorpion Relief.**

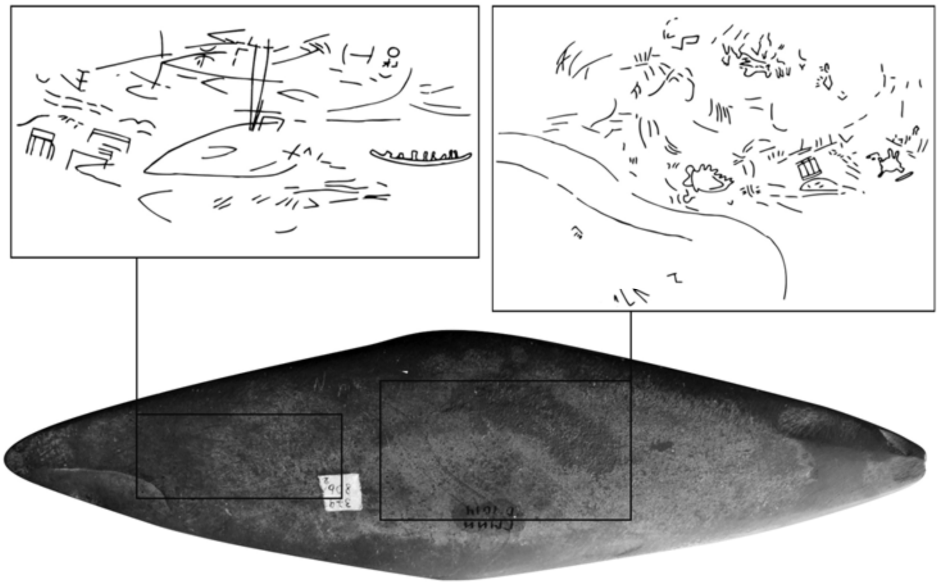

**Fig. 5 Fragments of signs on the Rhomboidal palette, LNMA, 379806.**

Characteristic stone surface alterations are easily recognisable on flat palettes that have been used for such purposes. Rhomboidal palettes, in turn, do not have such characteristic features as gentle deepening, more intensively used and irregularly treated surfaces and pronounced chemical weathering effects from the cosmetic compositions that should have been used for the purported aims. There are some exceptions, but their number is very small, and this prevailing lack of evidence is indicative of the use of rhomboidal palettes for symbolic ritual purposes rather than for mixing of cosmetic substances and subjecting them to the associated chemical and thermal impacts.

Rhomboidal palettes are not all alike, and their most typical shapes are known from Petrie's study, which also offers a simple classification according to the morphological features of these palettes (Plate LVIII) [2]. The shape of these palettes generally is reminiscent of a finely crafted stone axe, particularly a rhombic bifacial hand axe of a symmetrical design, thinner than usual, with meticulously treated surface. The skills of making ritual objects were very refined during that period of time, for example, the fine flint knapping skills represented by fragile flint figurines (well known from the HK6 cemetery) and leaf point pieces [8, 9]. This contrasts with the simplicity of images found on the palettes, indicating some different original meaning of the symbols.

The use of ancient stone tools or their copies as ritual objects is also known in Europe. Perhaps the

most well-known of such objects in Europe are the numerous variously-shaped carved stone artefacts from Skara Brae [10]. Although this object looks like an axe, in reality it could not be used for this or for other practical purposes, and this is confirmed by marks on its surface. Most likely, this object has some symbolic rather than decorative significance.

Similarly, rhomboidal palettes most likely had a ritual significance in the Naqadian culture of prehistoric Ancient Egypt. The external shape of these palettes is an indirect indication of this, while more direct indications are the fragments of ancient drawings depicting fishing scenes and various magical lines and stripes that are likely to have been made as parts of fortune and success symbols. Possibly, these symbolic tools were later decorated with new symbols, attesting to the rule of the king, its specific origin and meaning (for example, the palette with Scorpion Relief). Noteworthy, the later signs are made so that the earlier ones are not effaced completely, thereby emphasising the symbolic meaning of the tool.

It is known [8] that rhomboidal palettes were no longer made and used after the Naqada period. Also, there is no evidence of these palettes on vessel paintings and drawings on other objects. Presuming that there were no drastic changes in the way of life in this and the following period, of which we do not have any proofs, the ancient cults and items of religious significance should be traceable in some transformed form. Details of this transitional period from the Naqada period to the “00” and “0” dynastic periods in general indicate only gradual changes and accentuation of the role of the divine ruler. In the new symbols, the ancient gods, creators of the world can be recognised, and Ptah is among them.

Ptah as the creator of the world represents one of Ancient Egypt’s best-known cosmogony conceptions [11, 12] which endured for thousands of years, even through changes in many basic religious ideas and after the shift of interest from the past creation of the world to the future life after death. In the context of this study, Ptah is important not only as the creator of the world and embodiment of earlier periods of history but also due to his distinguishing token—a peculiar staff, particularly its hooked head. Most probably, the head of the staff (Was-sceptre) has a symbolic function for ancient cult participants.

This tradition has long been known and is also represented, for example, on the Narmer palette (plate), depicting ritual participants who carry poles with various symbols on their tops. Similar scenes are common in many ancient reliefs and drawings. This could be an explanation why the making of rhomboidal palettes was discontinued and they are not recognisable in subsequent periods: they became part of the symbols attesting to Ptah’s rule, and such symbols can be recognised throughout the subsequent historical periods of Ancient Egypt. Notably, one of the earliest known figures of Ptah is that on the Comb with the Name of Djet (Cairo Antiquities Museum, JE 47176). This artefact is from the period of the 1st Dynasty, when rhomboidal palettes were no longer made.

Testing of the aforementioned assumption can be simple—by finding out whether it is possible to affix such a rhomboidal palette on the top of a staff, so that it would be visible to cult participants. This question can best be answered by looking at the classification of rhomboidal palettes given by Petrie (Plate LVIII) [2].

It is obvious that the palettes 90L, 90H and 92M can be easily affixed on a staff’s top. Moreover, the palette 90H is remarkably similar in shape to the earliest images of Ptah’s staff. Accordingly, the explanation given in this paper can be taken as quite plausible. Also, from the visual point of view, for example, the Rhomboidal Palette from the Metropolitan Museum of Art (accession number: 10.176.82) is much more suitable for affixing on the tip of a staff than for uses with ritual offering or beauty care aims.

## 5. Conclusions

Perceptions of the Predynastic period of Ancient

Egypt have changed significantly over the past decades, and the long-known Badarian and Naqadian cultures are rightly considered as quite developed, with accomplished way of life and complex religious ideas. It was a time of many changes, of which we still do not know very much.

This is not the best time to study these cultures in Egypt, however, many museums all over the world have extensive and diverse collections of historical artefacts typical to the predynastic period that have not yet been studied adequately. Now, thanks to the digitalisation programmes of many museum collections, a vast scope of materials is made available for research.

Applying different kinds of image processing software and modifying and supplementing them with traditional manual methods, it is possible to obtain a bulk of new data for subsequent study in greater detail.

With this objective, it would be worthwhile to establish a centre for storing high-resolution images of stone palettes, known signs and their fragments that could serve as an archive and comparative data collection, facilitating the development of research and generation of new assumptions and hypotheses for further testing.

## References


[1] G. Brunton, G. Caton-Thompson, The Badarian Civilization and Predynastic Remains near Badari, British School of Archaeology in Egypt University College, London, 1928.

[2] W.M.F. Petrie, Corpus of Prehistoric Pottery and Palettes, British School of Archaeology in Egypt University College, London, 1921, p. 80.

[3] F. Raffaele, Corpus of Egyptian Late Predynastic Palettes [Online], 2013, http://xoomer.virgilio.it/francescoraf/hesyra/palettes.htm (accessed Dec. 24, 2013).

[4] D.K. Hitchin, Choice Museum Pieces [Online], 2013, http://egypt.hitchins.net/ancient-egytian-art/choice-museum-pieces.html (accessed Dec. 24, 2013).

[5] M. Mudge, J.P. Voutaz, C. Schroer, M. Lum, Reflection transformation imaging and virtual representations of coins from the hospice of the grand st. Bernard, in: M. Mudge, N. Rya, R. Scopigno (Eds.), Proceedings of 6th International Symposium on Virtual Reality, Archaeology and Cultural Heritage, VAST, 2005, pp. 29-39.

[6] T. Säve-Söderbergh, On Egyptian Representations of Hippopotamus Hunting as a Religious Motive, C.W.K. Gleerup, Lund, 1953, pp. 18-19.

[7] B. Midant-Reynes, The Naqada period (c. 4000-3200 BC), in: I. Shaw (Ed.), The Oxford History of Ancient Egypt, Oxford University Press, New York, 2003, pp. 41-56.

[8] W.M.F. Petrie, Prehistoric Egypt, British School of Archaeology in Egypt University College, London, 1920.

[9] E. Teeter (Ed.), Before the Pyramids, The Origins of Egyptian Civilization, Chicago Oriental Institute Museum, Chicago, 2011, p. 42.

[10] A. Sheridan, K. Brophy (Eds.), ScARF Neolithic Panel report, Scottish Archaeological Research Framework: Society of Antiquaries of Scotland [Online], 2012, http://www.scottishheritagehub.com/content/scarf-neolithic-panel-report (accessed Dec. 24, 2013).

[11] G. Hart, Egyptian Myths, University of Texas, Austin, Texas, America, 2004, pp. 1-2.

[12] R.H. Wilkinson, The Complete Gods and Goddesses of Ancient Egypt, Thames & Hudson, London, 2003, pp. 16-19.

Journal of Earth Science and Engineering 4 (2014) 101-106

# Relations between Low-Frequency Modes of Climate Variability and Air-Sea Heat Flux at the Mediterranean Interface

Lamri Nacef and Nour El Islam Bachari

*Department of Ecology and Environment, Faculty of Biological Sciences, Houari Boumediene University of Science and Technology, Algiers 16111, Algeria*

Received: December 02, 2013 / Accepted: January 17, 2014 / Published: February 25, 2014.

**Abstract:** The main objective of this work is to examine statistical causality relationships between low-frequency modes of climate variability and winter (December to February) anomaly of net heat flux at the Mediterranean air-sea interface. The introduction of the concept of Granger causality allowed us to examine the influence of these climates indices on the net heat flux anomaly and to select Mediterranean surface regions that really influenced by each index. Results show that the winter anomaly of the net heat flux in the Algerian basin south and the gulf of Lion is mainly caused by the Arctic Oscillation. El Niño-Southern Oscillation influences much more the Algerian basin north and the northern Ionian Sea. The Quasi-Biennial Oscillation affects only the Alboran and the Tyrrhenian Seas. But the Adriatic and Levantine basin are impacted by any climate index. They also show that these climate indices can increase explained variance in winter variations of air-sea net heat flux by 10% to 15%, with a lag of three seasons. These relationships are less persistent and spatially limited.

**Key words:** Mediterranean Sea, winter net heat flux, air-sea interface, climate index, causality analysis.

## 1. Introduction

Generally, the ocean-atmosphere interactions are dominated by atmospheric forcing which produces the SST (sea surface temperature) anomalies through the turbulent heat fluxes or the abnormal wind stress [1]. Alternatively, the ocean contributes to the dynamic of the atmosphere by the influence of SST anomalies and can generate afterward a persistent thermal forcing on the atmosphere [2-10].

The use of the simple correlation technique can distort the examination results of the causal order in highly associated systems such as, ocean-atmosphere. For example, the correlation between the winter NAO (North Atlantic Oscillation) and the previous seasons SST anomalies could be the result of persistence, or even the previous atmospheric anomalies affecting the SST during previous seasons. So, it is possible that the apparent signal of oceanic forcing is not provided solely by the ocean, but also by the atmosphere.

In this study, we introduced the concept of causality of Granger [11-13] to examine the possibility of whether or not there are relationships between the net air-sea interface heat flux in Mediterranean Sea and the low-frequency modes of climate variability with their causality order. The causality of Granger is based on the concept of predictability. With a coupled system involving two fields that inter-react reciprocally, the causality of Granger tests statistically if the previous values of the first field provide any more information about the second field. Variability in the first field is indicated as the cause of the variability in the second field.

**Corresponding author:** Nour El Islam Bachari, professor, research fields: modeling remote sensing, oceanography and sea environment, application of geographic information system methods in oceanology. E-mail: bachari10@yahoo.fr.

The variability of climate on global and regional scales is more characterized by the index of the AO (Arctic Oscillation), the QBO (Quasi-Biennial Oscillation) and ENSO (El Niño-Southern Oscillation) [14, 15].

As the variability of the air-sea interface heat fluxes in the Mediterranean Sea is higher in winter, winter anomalies (December to February) are used to analyze the relationship between the net heat flux at the Mediterranean air-sea interface and previous seasons climate indices.

In this paper, data are presented in Section 2. The methodology applied to test the causality of Granger is presented in Section 3 and the analysis results are described in Section 4. Conclusions and implications of the relationship between heat flux anomalies and climate indices are summarized in Section 5.

## 2. Data

The data of air-sea interface net heat flux in Mediterranean Sea are calculated on a monthly basis over the period of 45 years (1955 to 1999), in each 18 zones of the Mediterranean Sea surface (Fig. 1). This flux is obtained by integrating the monthly reconstructed temperature and salinity fields of the Mediterranean surface, extracted from the in situ MEDATLAS II [16] database. With these data, we are integrated the monthly data of air temperature at 2 m, dew point temperature at 2 m, clouds and wind components at 10 m, extracted from the ERA-40 re-analyzes.

Seasonal value is defined as the accumulated devalues of three successive months of the corresponding season. To eliminate the seasonal bias, the seasonal anomaly is standardized. And the seasons are defined as follows: MAM (March to May) for spring, JJA (June to August) for the summer, SON (September to November) for the autumn and DJF (December to February) for the winter.

Over the same period (1955 to 1999), the normalized monthly climate indices are extracted from CPC/CDC–NOAA/USA.

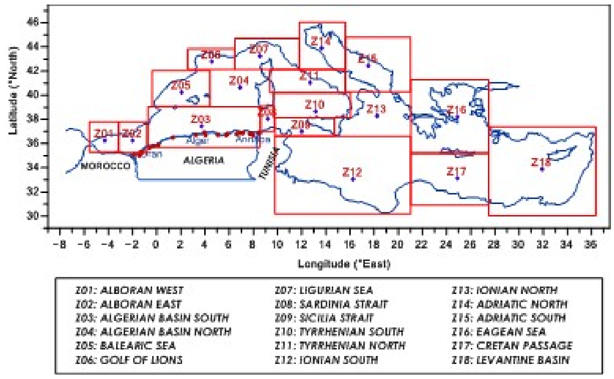

**Fig. 1 Study area, defined by a grid of 18 spatial points (each point represents a sub-region of the Mediterranean Sea surface).**

The seasonal indices of *AO* and *ENSO* are calculated by averaging the three monthly indices in the corresponding season. The extracted *QBO* index data are not normalized, the monthly anomaly is normalized and the seasonal index is calculated by averaging the three monthly normalized anomalies in the corresponding season.

## 3. Methodology

Examination of Granger causality presence between the net heat flux anomalies at the air-sea interface in the Mediterranean Sea ($Q_{net}$) and each climate index (AO, *QBO* and *ENSO)* is performed according to the procedure used by Kaufmann and Stern [17] and by Mosedale et al. [12]. This procedure involves two steps: In the first one, bilateral interactions between the winter (DJF) net heat flux anomaly in each 18 areas of the Mediterranean Sea (Fig. 1) and the previous seasons climate indices are described by varying the regression coefficients with the shifting seasons and using an auto-regression vector given by the following equation :

$$Q_{net_{DJF}} = \alpha_2 + \sum_{i=1}^{s} \beta_{2i} I_{DJF-i} + \sum_{i=1}^{s} \gamma_{2i} Q_{net_{DJF-i}} + e_{2_{DJF}} \quad (1)$$

where

$I$: Seasonal climate index (e.g., AO);

$Q_{net}$: Seasonal net heat flux anomaly;

$\alpha_2, \beta_2$ and $\gamma_2$: The regression coefficients;

$e_2$: The error term;

$s$: The number of seasonal shifted.

The values of winter $Q_{net}$ in Eq. (1), corresponding

to each of the 18 zones are based on the three previous seasons values of the climate index, indicated by the first sum and $Q_{net}$ values in the three past seasons indicated by the second sum in Eq. (1).

To determine the direction and causality order, i.e., to test whether or not the variability of the previous seasons climate index causes the winter $Q_{net}$ variability, we consider a restricted form of Eq. (1) in which we eliminate the past values of the climate index. This is statistically done by taking $\beta_2 = 0$ in Eq. (1) as follows:

$$\boldsymbol{Q_{net_{DJF}}} = \boldsymbol{\alpha'_2} + \sum_{i=1}^{s} \boldsymbol{\gamma'_{2i} Q_{net_{DJF-i}}} + \boldsymbol{e'_{2_{DJF}}} \quad (2)$$

where

$Q_{net}$: Seasonal net heat fluxanomaly;

$\alpha'_2$ and $\gamma'_2$: The regression coefficients;

$e'_2$: The error term;

$s$: The number of seasonal shifted.

The second step is to statistically test if the estimations of the restricted form (Eq. (2)) are significantly different from that of the unrestricted form (Eq. (1)). To do so, we calculate the statistic test as follows:

$$\omega = \frac{\frac{(RSS_r - RSS_u)}{s}}{\frac{RSS_u}{(T-k)}} \quad (3)$$

where:

$RSS$: The sum of squared residuals;

$r$ $and$ $u$ : Denote respectively to the restricted version and unrestricted one;

$T$: Number of observations;

$k$: The number of independent variables in the version without restriction ($k = 2s + 1$);

$s$: The number of coefficients returned to zero in (Eq. (2)).

The statistic $\omega$ is evaluated according to the Fisher distribution (F) at 5% of the threshold with $s$ and $T$-$k$ degrees of freedom. The acceptance of the test means that climate variability does not cause variability in winter $Q_{net}$ anomaly. If the test result is a rejection, we conclude that the climate index causes the variability of winter $Q_{net}$ anomaly.

A significant increase in $RSS_r$ indicates that the elimination of the climate index values reduces the explanatory skill of the autoregressive vector and increases the sum of squared residuals. So, the statistic $\omega$ measures the information contained only in the past climate index values and represents the statistical robustness force of the Granger causality compared to the simple correlation technique.

Also, the correlation analysis between the winter net heat flux anomaly (DJF $Q_{net}$) in each 18 zones of the Mediterranean Sea surface and each previous season climate index (autumn, summer and spring) is performed to observe the degree of consistency between the two techniques.

## 4. Results and Discussion

The correlation analysis results show that the links between each previous seasons climate index and the winter air-sea interface net heat flux in the Mediterranean sea is weak and spatially limited (Fig. 2). Indeed, the spring AO index (Fig. 2a) is significantly correlated with winter $Q_{net}$, only in the Algerian basin south ($r = 0.35$). Excepting the Aegean Sea, the winter net heat flux anomaly is negatively correlated with the Quasi-Biennial Oscillation (Fig. 2b). Though, this correlation is significant only in the Alboran Sea with a maximum correlation ($r = -0.47$), achieved between winter $Q_{net}$ and summer QBO. Concerning ENSO index, Fig. 2c shows no significant correlation with the winter anomaly $Q_{net}$, however, presents relatively more high correlations in the western Mediterranean Sea.

Considering the lag at one season (previous autumn), at two seasons (previous summer) and at three seasons (previous spring), Fig. 3 shows the results of Granger causality tests. The ($r_u^2 - r_r^2$) values represent the difference between the determination coefficient ($r^2$) statistics, corresponding respectively to the version without restriction (Eq. (1)) and the restricted version (Eq. (2)). It describes the portion of information quantity provided by the previous

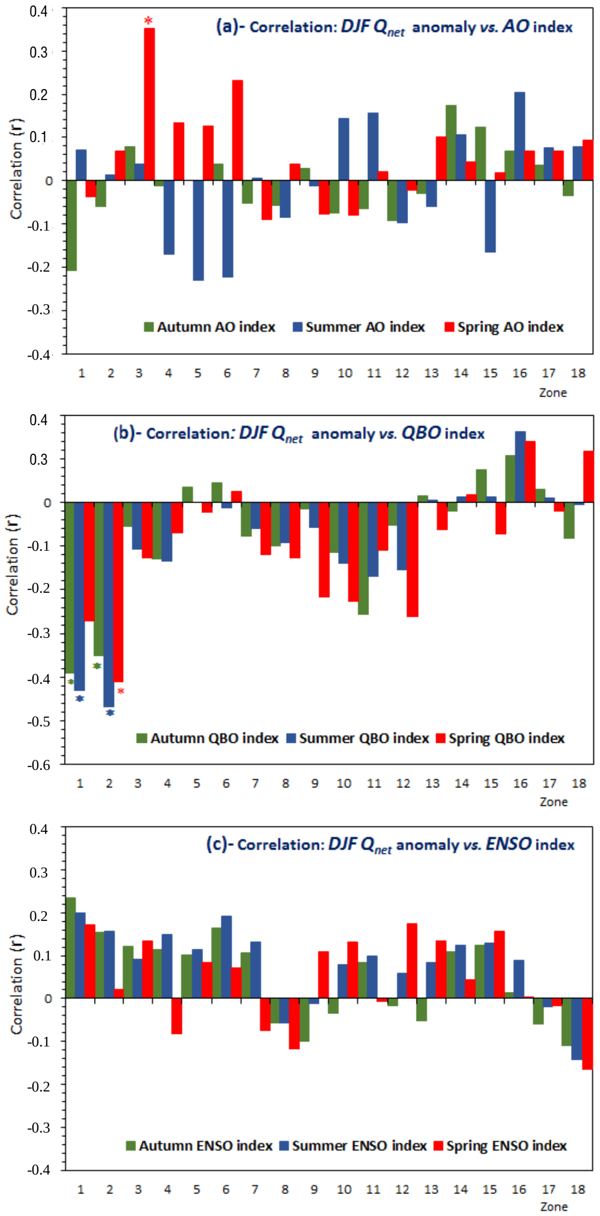


**Fig. 2 Correlations ($r$) between winter air-sea interface net heat flux anomaly in Mediterranean Sea and each previous season climate indices.**

* indicates that the correlations are statistically significant at 5% of the threshold.

season climate index to explain the winter $Q_{net}$ variance.

These results show that variations in the previous spring AO index cause significantly the variations in the winter net heat flux $Q_{net}$ in Gulf of Lion, in the Algerian basin south and in the southern Tyrrhenian Sea. Whereas, in the rest of the Mediterranean Sea surfaces, there is no statistical evidence for a causal

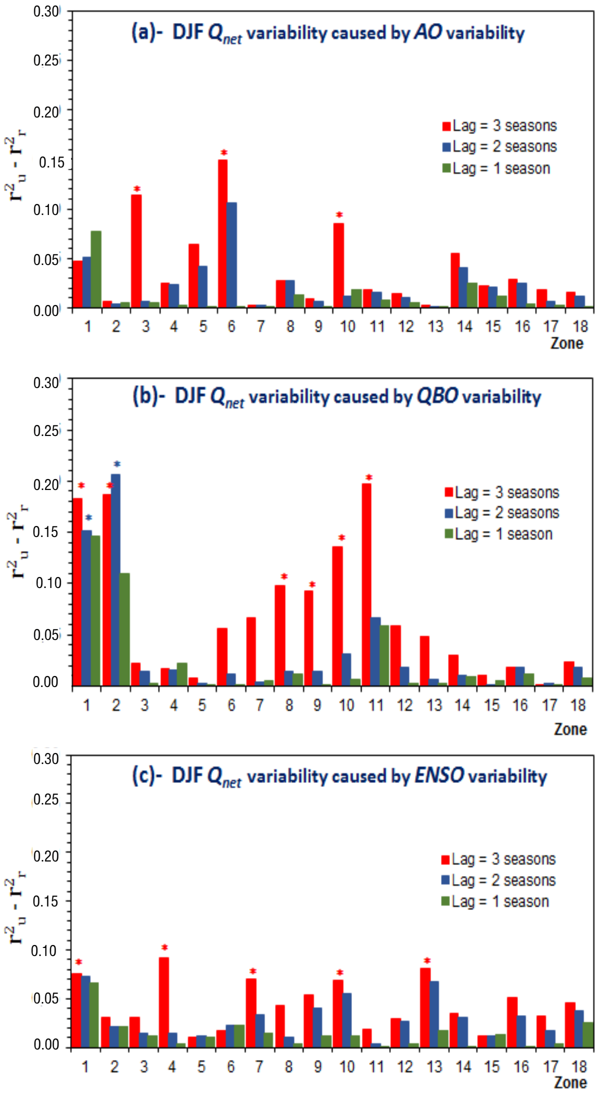


**Fig. 3 Granger causality analysis: winter $Q_{net}$ variability in each 18 zones of the Mediterranean Sea surface caused by climate indices (*AO*, *QBO* and *ENSO*) of the previous three seasons.**

* indicates that the $(r_u^2 - r_r^2)$ values are statistically significant at 5% of the threshold.

influence of AO on net heat flux (Fig. 3a). These relations are in agreement with the maximum positive correlations between winter $Q_{net}$ and spring AO index. In these three zones, the $(r_u^2 - r_r^2)$ values indicate that spring AO index reduces the succeeding winter $Q_{net}$ unexplained variance by 9% to 15%. Furthermore, with the reduction of the temporal lag, the AO influence on winter $Q_{net}$ decreases and becomes insignificant. Thus, the previous seasons AO index do not contain enough explanatory information

about the winter air-sea interface net heat flux in Mediterranean Sea, except for the Lion golf and Algerian basin south.

Conversely to the AO index, the variation in the previous seasons QBO index cause variations in the winter net heat flux in well-defined regions, which are the Tyrrhenian and the Alboran Seas (Fig. 3b). Indeed, the spring QBO index variation can increase the explanatory skill of following winter $Q_{net}$ variations by 18% to 19% in Alboran Sea and 14% to 20% in Tyrrhenian Sea, while the summer QBO index variation can increase the explanatory skill of succeeding winter $Q_{net}$ variations by 15% to 21% in the Alboran Sea. These sea surface regions correspond to the maximum negative correlations between winter $Q_{net}$ and QBO index (maximum correlation is achieved between winter $Q_{net}$ and QBO index of SON and of JJA). Apart from these two regions, the results indicate no statistically significant causal influence of QBO index on the net heat flux in the rest of the Mediterranean Sea surface.

Fig. 3c shows that the variations in the spring ENSO index cause variations in the following winter net heat flux, in localized and dispersed areas. They influence the net heat flux in the western Alboran Sea, in the Algerian basin north, in the Ligurian Sea, in the southern Tyrrhenian and in the northern Ionian Seas. Moreover, there is no statistical certainty about a causal influence of autumn and summer ENSO index on winter net heat flux. In the zones where there is a significant causality, ($\mathrm{r}_u^2 - \mathrm{r}_r^2$) values indicate that the past spring ENSO index reduce the unexplained variance only by 7% to 9% and the ($ENSO_{MAM} - Q_{net_{DJF}}$) relationship is stronger in the Algerian basin north.

Although the results obtained by Granger causality and those by simple correlation analysis are quite coherent, we note that such an agreement does not always appear, for example, the autumn QBO index is significantly correlated with winter $Q_{net}$ in the Alboran Sea ($r$ = -0.39; Fig. 2b), but when the technique of Granger causality examines the influence of the autumn QBO index on following winter $Q_{net}$ anomaly. Fig. 3b shows that this correlation is really related to the autumn $Q_{net}$ anomaly field itself (the persistence result) and therefore cannot be attributed to the previous seasons QBO indices. So the technique of Granger causality is stricter and more reliable than the simple correlation.

## 5. Conclusions

The use of the concept of Granger causality allowed us to examine the relationships between the modes of climate variability (climate indices) from previous seasons and the winter net heat flux anomaly at the Mediterranean air-sea interface.

The obtained results show that the influence of each climate index from previous seasons on the winter net heat flux is spatially limited and significant causal relationships are weak and not much persistent. In average, the relative variation in each spring climate index can increase the explanatory skill of variations in the following winter net heat flux by 10% to 15%. The winter anomaly of the net heat flux in the Algerian basin south and the Gulf of Lion is mainly caused by the Arctic Oscillation. The ENSO index influences or affects much the Algerian basin north and the northern Ionian Sea, while the QBO influences or affects only the Alboran Sea and the Tyrrhenian Sea. Contrariwise, the Adriatic and the Levantine sea surfaces are influenced by any climate index. These results are in agreement with those of the correlation analysis. However, the Granger causality is a more rigorous test for the causal order in a coupled system.

Although these results are based on statistics and are limited by the schema approach, these three climate indices in particular, AO and QBO can be used as Proxy (predictors) to improve the prediction of winter net heat flux air-sea interface variations in some areas of the Mediterranean Sea.

## References

[1] D.R. Cayan, Latent and sensible flux anomalies over the

northern oceans: The connection to monthly atmospheric circulation, Journal of Climate 5 (1992) 354-369.

[2] Y. Kushnir, W.A. Robinson, I. Bladé, N.M.J. Hall, S. Peng, R. Sutton, Atmospheric GCM response to extra-tropical SST anomalies: Synthesis and evaluation, Journal of Climate 15 (2002) 2233-2256.

[3] W. Wang, B.T. Anderson, R.K. Kaufmann, R.B. Myneni, The relation between the north Atlantic oscillation and SSTs in the north Atlantic basin, Journal of Climate 17 (2004) 4752-4759.

[4] S. Conil, Z.X. Li, Linearity of the atmospheric response to north Atlantic SST and sea ice anomalies, Journal of Climate 18 (2005) 1986-2003.

[5] D. Bourras, G. Caniaux, H. Giordani, G. Reverdin, Influence d'un tourbillon océanique sur l'atmosphère (The influence of currents on the atmosphere), La Météorologie 53 (2006) 30-37.

[6] W. Wang, B.T. Anderson, N. Phillips, R.K. Kaufmann, Feedbacks of vegetation on summertime climate, Variability over the north American grasslands, Earth Interactions 10 (1) (2006) 10-17.

[7] Z.X. Li, Atmospheric GCM response to an idealized anomaly of the Mediterranean Sea surface temperature, Climate Dynamics 27 (2006) 543-552.

[8] C. Deser, R.A. Tomas, The transient atmospheric circulation response to north Atlantic SST and sea ice anomalies, Journal of Climate 20 (2007) 4751-4767.

[9] D. Ferreira, C. Frankignoul, Transient atmospheric response to interactive SST anomalies, Journal of Climate 21 (2008) 576-589.

[10] B. Fontaine, J. Garcia-Serrano, P. Roucou, B. Rodriguez-Fonseca, T. Losada, F. Chauvin, et al., Impacts of warm and cold situations in the Mediterranean basins on the West African monsoon, Climate Dynnamics 35 (2010) 95-114,

[11] C.W.J. Granger, Investigating causal relations by econometric models and cross-spectral methods, Econometrica 37 (1969) 424-438.

[12] T.J. Mosedale, D.B. Stephenson, M. Collins, T.C. Mills, Granger causality of coupled climate processes: Ocean feedback on the north Atlantic oscillation, Journal of Climate 19 (2006) 1182-1194.

[13] D.D. Zhang, H.F. Lee, C. Wang, B. Li, Q. Pei, J. Zhang, et al., The causality analysis of climate change and large-scale human crisis, in: Proceedings of the National Academy of Sciences of the USA, 108, 2011, pp. 17296-17301.

[14] K. Kodera, Y. Kuroda, Two teleconnection patterns involved in the north Atlantic/Arctic oscillation, Geophysics Research Letter 31 (2004) 20198-20201.

[15] D.W.J. Thompson, J.M. Wallace, The arctic oscillation signature in wintertime geopotential height and temperature fields, Geophysics Research Letter 25 (1998) 1297-1300.

[16] MEDAR Group, MEDATLAS/2002 database, Mediterranean and Black Sea database of temperature salinity and bio-chemical parameters, Climatological Atlas, 2002 [CD-ROM].

[17] R.K. Kaufmann, D.I. Stern, Evidence for human influence on climate from hemispheric temperature relations, Nature 388 (1997) 39-44.

Journal of Earth Science and Engineering 4 (2014) 107-112

# Study of Effective Ingredient on the Landslides of Isfahan Province

Mojgan Entezari and Somayeh Sadat Shahzeidi

*Engineering Research Institute of Natural Disaster of Shakhes Pajouh, College of Geographical Science and Planning, University of Isfahan, Isfahan 8174673441, Iran*

Received: July 29, 2013 / Accepted: August 25, 2013 / Published: February 25, 2014.

**Abstract:** Usually landslide studying investigates the facts such as gender land, atmospheric rainfall, gradients' change, earthquake, volcanic eruption, subterranean water vibration, and human causes in the form of different models. However, the facts can have main share in appearing this phenomenon but correlative and sufficient condition for genesis and such a phenomenon is historical base of lands' bed that has experienced specific formative process. In the case of distribution and dispersion of slides and their reasons of occurring in Isfahan, general studying has also been carried out. And this article has investigated this phenomenon on the other aspects and has tried to reveal this phenomenon's effect on instigating instabilities, so that it can conclude distribution of this phenomenon references to climate on one side and historical formative process on the other side. It aims to study this effect by using IDW (Inverse Distance Weighting), Kiriging method in ArcGIS 9.3 software dispersal map of Isfahan's main landslides and formative systems on the other side and by local analyzing these two collections evaluated their vicinity relation using local-statistical ways. Results of this research will show that in the past the main part of this landslide has occurred in cold hole and seldom occurred in hot hole.

**Key words:** Landslide, cold hole, hot hole, climatic formative system, IDW, Kiriging method.

## 1. Introduction

Geomorphologic studies show that there is an organic relationship between climate and landforms of earth. This relationship is so high that the geomorphology scientists believe that geomorphologic phenomena are acquired through internal and external formation power [1].

The appearance of most of external geomorphologic phenomena depends on various climatic zonal. Although, climate has significant role in the creation of geomorphic forms and their changes during time, but all of the climates can not affect on geomorphic changes. In other words, weight and combination of determined parameters in each climate must reach the level in which climate enable to landform [2]. Landslide is one of the geomorphologic phenomena affected by formative systems. Landslide is a mass movement of the founding materials of earth in a slope from higher level to the lower level [3].

Many researchers tried to present models for zoning of landslide hazard. In other words, they wanted to reach the map of landslides' zoning based on inductive method. They investigated different effective factors in the slides occurrence and their effects on the distribution of slides. However, in this paper, the authors used deductive method to reach the details from the whole and also used the formative systems, cold and hot holes related temperature which limits to predict and determine the zoning of landslide hazard. The terms—hot and cold holes—are derived from hot and cold pool of air in climatology [1]. In geomorphology, these regions are different from hot and cold holes. Hot and cold holes against hot and cold

**Corresponding author:** Mojgan Entezari, assistance professor, research field: geomorphology. E-mail: entezary54@yahoo.com.

pools are fixed spatially, and also they depend on the geomorphologic structure of the region.

## 2. Background of the Study

There are many different studies about the effects of climatic changes on slide occurrence. Claude et al. [4] studied the slides of south of France, indicating that there is a good interrelationship between climatic change and landslide, although the amount of this interrelationship depends on type and time of slide occurrence. Also, Martin et al. [5] investigated the slides' sediments in east of Chloride, stating that most of mass movements occurred in two periods during quaternary. The oldest groups of slides occurred in moisture era and in equatorial and semi-equatorial regions in south of America. Entezari [6] contemporary with the researches of Ireland geology organization on the slides in south of Europe and Ireland expressed that climatic changes result in mountainsides' instability and also prepare an appropriate condition for slide occurrence.

## 3. Methodology

First of all, the authors of this paper investigated the air photographs and field studies to find the place of 619 landslides in Isfahan on DEM (digital elevation model) of province using Software ArcGIS 9.3 (digital altitudinal model with 85 m cellular size gained from the digital photos of radar). In order to determine the position of hot-cold centers in province, the statistics of 93 climatic and synoptic stations of Isfahan and neighboring provinces were investigated and analyzed. Among these stations, the stations with temperatures 5 °C or under 5 °C during three or four months called cold stations.

The average of three cold months in cold stations were calculated for the statistical period and then the map of formative systems were prepared by Inverse Distance Weighting, Kiriging method and comparison between them and using Software ArcGIS 9.3 in Isfahan. Finally, after overlapping these maps with distributive map of slides, calculating the extent of hot and cold zones by IDW, Kiriging method and number of occurred slides, the percentage of occurred slides in each region were determined and analyzed. After integrating these two maps, the conditions were prepared to analyze the place of slide occurrence and its relationship to hot and cold cells. Then, creating proportion between number of slides and the extent of climatic zones and calculating index *I*, the effects of these zones on the slides occurrence were compared in past and present.

### *3.1 Hot-Cold Holes in Isfahan*

In order to create a spatial numerical models for hot-cold center by IDW and Kiriging method, the average temperature of meteorological datum of 93 climatologic and synoptic stations in Isfahan and neighboring province was extracted and also it was considered a hot season and a cold season for each station regardless of periodic range of recording the datum in the station. Fifty-one stations out of these stations were called cold stations in which their temperatures were lower than or equal to 5 °C during three months to four months. Seventeen stations among these stations are located in the limitation of Isfahan province (Fig. 1).

### *3.2 Relationship between Slides and Formative Systems*

As mentioned before, based on climatic formative systems, Isfahan was classified into different regions. Regarding temperature, moisture and rainfall, each of these systems has special characteristics. These characteristics present independent formative framework, somehow it can explain the differences of morphology in the area of these systems. Moreover, these formative systems have special dynamic relationships with each other which can be clarified in the cyclic and seasonal scale. If numbers of slides are divided on the extent of formative systems in each periodic era, the index *I* will be calculated based on Eq. (1).

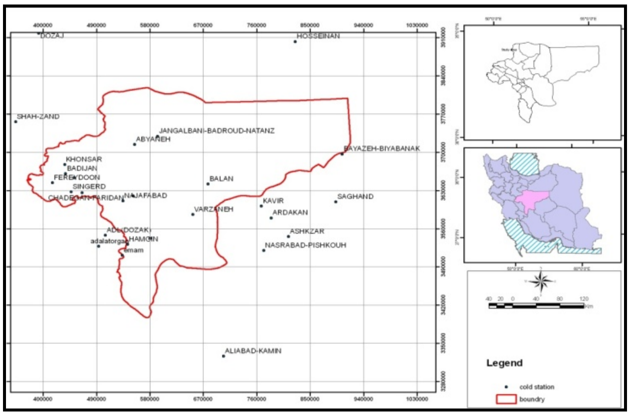


**Fig. 1 Location of 17 cold stations of Isfahan province.**

$$I = \frac{NI}{AZ}$$

where *I* = landslide index; *NI* = No. of landslide; *Az* = area of formative system.

The investigation of this index and calculation of slides' percentage in each formative systems with two methods show that (cold phase of quaternary) in the past, there was a little different between the size of hot and cold holes in the province, but in the IDW method about 92% and in the Kiriging method about 100% slides occurred in the limits of cold holes (Tables 1 and 3). At present, contemporary with the occurrence of hot phase of quaternary, the size of hot holes increases and the size of cold holes decreases in two methods (Figs. 2-5). However, the percentage index of slides in cold hole in the IDW increased from 92% to 95% (Tables 1 and 2) and in the Kiriging decreased from 100% to 74% (Tables 3 and 4). It is considerable that this limits whatever in past located in cold holes. At the present it locates in the limitation of hot holes and in this limit it emerges maximum slides. You can find more explanations in the following.

Generally, mass and mountainside movements are classified in different groups based on their founding materials, type of movements, speed and the size of activity. According to these classifications, the movements include two groups: vertical and lateral groups and each group is divided into minor group respectively [7]. The main groups of these movements involve slide, mountainside fall, creep, cell flexion and mud flow [3]. One of the most primary fields for falling and sliding is the mechanical destruction of rocks which can occur in cold centers. Mechanical destruction relates to the changes of temperature. Because of changes of temperature, the rocks are extended and contracted and then they cracked. This process called Thermoplastic [8]. It is not so important, when temperature rises higher than 0 °C, but the

**Table 1 Percentage of slides occurrence in each formative system in the past (cold phase) IDW.**

| | No. of landslides | Index % | Index *NI*/*Az* | Area (ha) |
|---|---|---|---|---|
| Hot holes | 54 | 7.8 | 0.000006 | 5,693,686 |
| Cold holes | 560 | 92.2 | 0.00011 | 5,008,932 |

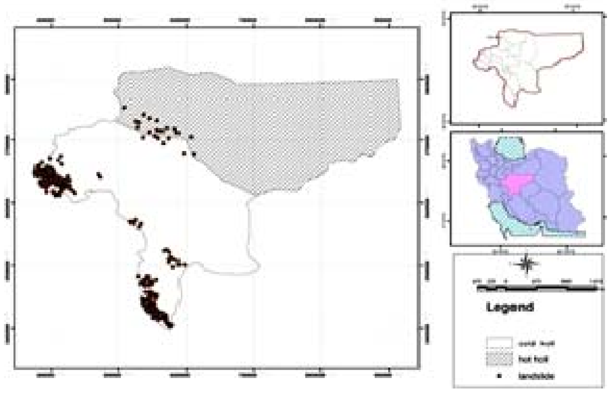


**Fig. 2 Distribution of slides in hot and cold holes in the past IDW.**

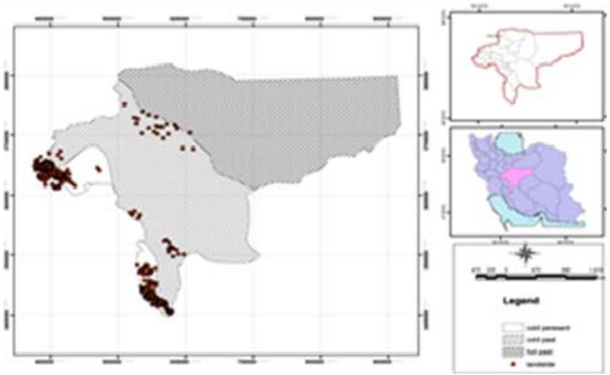


**Fig. 3 Distribution of slides in hot and cold holes in the present IDW.**

**Table 2 Percentage of slides occurrence in each formative system in the present (hot phase) IDW.**

| | No. of landslides | Index % | Index *NI*/*Az* | Area (ha) |
|---|---|---|---|---|
| Hot holes | 255 | 5 | 0.0000025 | 9,951,360 |
| Cold holes | 364 | 95 | 0.00048 | 751,258 |

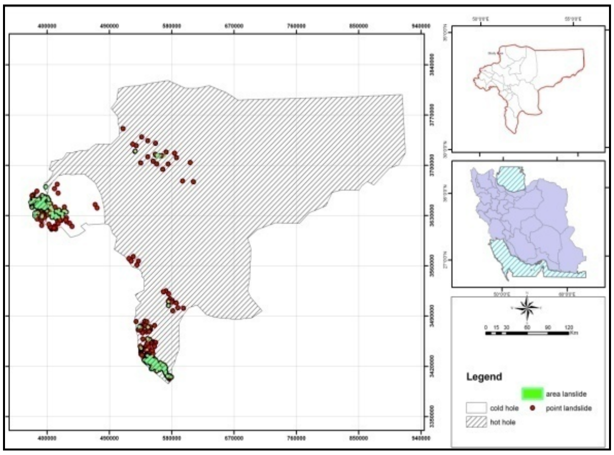


**Fig. 4 Distribution of slides in hot and cold holes in the present Kiriging.**

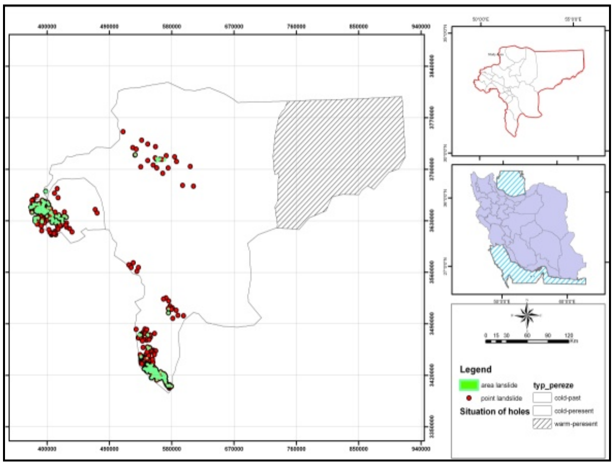


**Fig. 5 Distribution of slides in hot and cold holes in the past Kiriging.**

**Table 3 Percentage of slides occurrence in each formative system in the past (cold phase) Kiriging.**

| | No. of landslides | Index % | Index *NI/Az* | Area (ha) |
|---|---|---|---|---|
| Hot holes | 0 | 0 | 0 | 2,524,469.4 |
| Cold holes | 619 | 100 | 0.00007 | 8,189,921.5 |

**Table 4 Percentage of slides occurrence in each formative system the present (hot phase) Kiriging.**

| | No. of landslides | Index % | Index *NI/Az* | Area (ha) |
|---|---|---|---|---|
| Hot holes | 534 | 26 | 0.000052 | 10,133,115.6 |
| Cold holes | 85 | 74 | 0.00014 | 567,294 |

freezing phenomenon is the key factor of falling rocks. In 1965, Rapp demonstrated when temperature rises up from the degrees under zero to the upper degrees, it can be an important factor in falling rocks. As you know, almost all of rocks which are appeared on the earth partly have various small and big hole, crack and seam. When it is raining, some water penetrates into the rocks easily. If raining is heavy and steady, most of the holes are saturated by water. When water is freezing inside the rocks, its volume increases up to 10% and the rock breaks into pieces. The rocks disintegrating and shattering depends on many factors, such as, porosity, size of cracks in the rock and other physical characteristics like texture and structure of rock. It can create different mass movements.

After arriving interglacial era (summer of earth) and increasing temperature, the expansion of hot centers districts the cold ones. Settling hot cell on top of Iran, temperature increases in whole country especially in Isfahan, cold centers decrease and create only in the latitudes and finally hot centers become fixed. Quick cold or humid changes develop special morphed forms based on dominated formative system in the area. For instance, quick changes of temperature in continents especially in the slopes of mountains caused to melt the ice resources, to flow a huge energy of water and to prepare an appropriate condition for slides occurrence in these areas in a few time.

Therefore, it is considerable that the effects of momentary and quick changes on formative systems are different from the effects of permanent, constant and slow changes. In slow changes, environment always can be adapted by the new conditions. During these kinds of changes, formative systems often are changed completely and produced special geomorphologic phenomenon on the external surface of earth. In other words, each of them is an evidence for the dominated formative system or is a climatic system. The existence of each of mentioned era in Iran develops a special formative system and their effects can be traced and recognized as geomorphologic evidences and outlooks. Because of developing hot centers and increasing temperature, in the place of cold centers in which the glacial systems were activated, another system substituted with the glacial system. Increasing temperature caused snow boarders

rise to the higher areas and glacial lateral systems were activated instead of them.

Main mechanism in glacial lateral systems includes constant freezing and melting. Freezing is so weak in dry environments but so strong in humid environments. In humid environments, water penetrates into the rocks and sediments well, when the temperature is below zero, they are freezing and their volumes are increasing and finally the rocks are cracking and the soil is puffing. While ice is melting, the pieces of rocks which were connected to each other by ice separated and fell. Totally, most of slides and falls occurred during melting [9]. Water produced by melting and deep sediments of freezing saturated the soil and produced a special kind of solifloxin which is called gelifloxin (material movement like a cloyed in glacial environments). This movement occurred when the soil was saturated by water completely, because soil freezing prevents from penetrating water to the lower levels. Ice and snow melting saturated the lands of this area and caused soil flow on the surface of soil [10].

## 4. Summary and Conclusion

According to the investigation on the effective factors in slide occurrence, it is evident that recognizing the area prone to slide is one of the most important methods of preventing and decreasing losses caused by this phenomenon. One of the main points about the distribution of landslides in Isfahan is that these forms follow and affect stellar climatic areas as a symbol of formative identical characteristic. The results show that in Isfahan, there are only two hot and cold systems out of four climatic formative systems in Iran, which have two different extents previously and presently. Presently, the extent of hot holes increases to 4,257,674 ha and also the same amount of extent of cold hole decreases.

While the index of slide shows that percentage of this index in cold hole in the IDW method in the present is about 95% and in the Kiriging method is 74%. Main effective factors in this kind of slide occurrence include sudden changes in temperature, extension and contraction of rocks, freezing water in cracks and seams of rocks. Also, maximum slides regardless of their extents were located in the limitation of cold holes in the past, but now they are located in the limits of hot holes. Its cause is linked to thermodynamic relationships between hot and cold centers. In cold season equal to glacial era, almost half of Isfahan was surrounded by the cold holes. These areas were affected by glacial system. Sediments were freezing deeply and rocks cracking because of changes in temperature and freezing water in cracks and streams.

When hot season, equal to interglacial era, begins, hot interrelationships between hot and cold holes will cause contraction in cold holes and extension in hot holes. Somehow a large extent of areas is located in the limits of cold holes, developing to the limits of hot holes. These changes in temperature resulted in the changes of glacial systems into glacial lateral systems and finally melted sediments saturated soil by water and developed a huge amount of mass movements of slides such as solifloxin and gelifloxin. Seldom slides are evident in hot centers. These slides usually occurred for many reasons such as: tectonic factors like earthquake and physiological factors. In sum, density of slides in these areas is low because of reasons like changes of temperature, slope and lithology.

## References

[1] G. Zomorodian, Geomorphology of Iran, Climatic and external dynamic processes, Ferdosi University of Mashad, 2002.

[2] A. Abbasi, Spatial and genetic analysis of cone shaped of Iran, Ph.D Thesis, Islamic Azad University of Najaf Abad, 2008.

[3] M. Ramesht, N. Shoshtari, Icing zone works and glacial effects in Salafchegan, Qom, Geographical Studies (2005) 119-132.

[4] J. Claude, F. Maquaire, B. Martin, D. Weber, Landslides and climatic conditions in the Barcelonnette and Vars

basins (southern French Alps, France), Elsevier Science, Geomorphology 30 (1-2) (1999) 65-78.
[5] H. Martin, T. Ricardo, A. Kirk, R. Haselton, Climate change and mass movements in the NW Argentine Andes, Earth and Planetary Science Letters, Vol. 179, Issue 2, 2000.
[6] M. Entezari, S. Shahzeidi, The impacts of formative system on the landslides of Iran, Management Science, Letters 2, 2012, pp. 945-950.
[7] D.J. Varnes, Slop movement type and processes, in: R.L. Schster, R.J. Krizek (Eds.), Special Report 176 Landslide: Analysis and Control, TRB, National Research Council, Washington, 1978, pp. 11-33.
[8] M.A. Carson, M.J. Kirkby, Hill Slope Form and Process, Cambridge University Press, Cambridge, England, 1972.
[9] A. Rapp, Recent development of mountain slopes in Karkevagge and surroundings, northern Scandinavia, Geografiska Annaler 42 (1960) 71-200.
[10] R. Chorley, Sh. Stanly, S. David, Geomorphology (translated by A. Motamed), 3rd ed., Samt Pub., Tehran, 1996.

Journal of Earth Science and Engineering 4 (2014) 113-120

# Trace Metals (Cu, Pb, Zn, Mn, Mo, As) Analysis as a Base for Environmental Studies in Argentina

Adolfo Antonio Gutiérrez and Ricardo Mon

*Faculty of Natural Sciences and Miguel Lillo Institute, National University of Tucuman, San Miguel de Tucumán 4000, Argentina*

Received: September 09, 2013 / Accepted: Octomber 20, 2014 / Published: February 25, 2014.

**Abstract:** In Argentina, at Central Andes Eastside, Cumbres Calchaquíes, Aconquija Range and Ambato Block constitute a mountain chain that erects about 5,000 masl. Its geological story reveals morphotectonic and magmatic processes are similar to the Pampean Ranges at which they belong to, giving origin to mineralized areas. Geochemical concentrations of trace metals (Cu, Pb, Zn, Mn, Mo, As) in stream sediments are related to the geology and mineral manifestations of the area. Geochemical high average concentration of Cu, Pb and Mo are observed in all ranges. It highlights the presence of As in Cumbres Calchaquíes-Aconquija Range and Zn, Mn in the mountains of Aconquija Range-Ambato Block. It was determined that Cu-Zn-Mn complex is adsorbed or precipitated most frequently by Mn oxides. Complex Pb-Zn, Mn-As, Mo-As and Pb-Mo are absorbed by other agents (clay; oxides of Mn, Fe, Al; organic matter).

**Key words:** Geochemistry, trace metals, Andean, Pampean Ranges, environmental.

## 1. Introduction

Cumbres Calchaquíes, Aconquija Ranges and Ambato Block northern area in the border of Tucumán and Catamarca provinces (Fig. 1) divided the superficial draining into three watersheds. Salado River basin converges to Paraná River, Dulce River basin converges to Mar Chiquita Lagoon and Colorado River basin converges to La Rioja plains (Fig. 2). In the northwestward, drainage network converges in Santa María River, a tributary of Salado River (Fig. 2). In the southwestward, draining download in Pipanaco Salt flat and Valley River, Colorado River tributaries (Fig. 2). Salí-Dulce River is the main collector that drains to the East, to Mar Chiquita Lagoon (Fig. 2).

The orographic chain formed by Cumbres Calchaquíes, Aconquija Range and Ambato Block reaches 5,500 masl and constitutes a climatic barrier to easterly winds. On the eastern slope of the mountain range, the rainfalls reach 2,000 mm every year; but to the west, register suddenly drop at 200 mm annual.

Mayor cities are located in the western and eastern foothills of the mountain ranges and other minor population occupies intermountain valleys. In the northern of the Tucuman province, livestock activity and milking yards are highlighted. Agricultural activities include the production of vegetables, bilberry, beans, walnuts, fodder, sugar canes, citric, tobacco, potato, soja, etc.. In Tafi Del Valle, potato, beans, strawberry and fodder agriculture prevail over livestock production, as well as in the intermountain valley in Ambato Block. In Santa Maria Valley, Catamarca, wine industry stand out due to vine farming (Fig. 1).

In close relationship with aquifer systems and the superficial draining, the chemical elements found in minerals that constitute rocks and soils determine the chemical content and water quality draining from the geological environment, with direct implication in

**Corresponding author:** Adolfo Antonio Gutiérrez, Ph.D., geologist, research fields: tectonic, economic geology and geochemistry. E-mail: gutierrez.aa@hotmail.com.

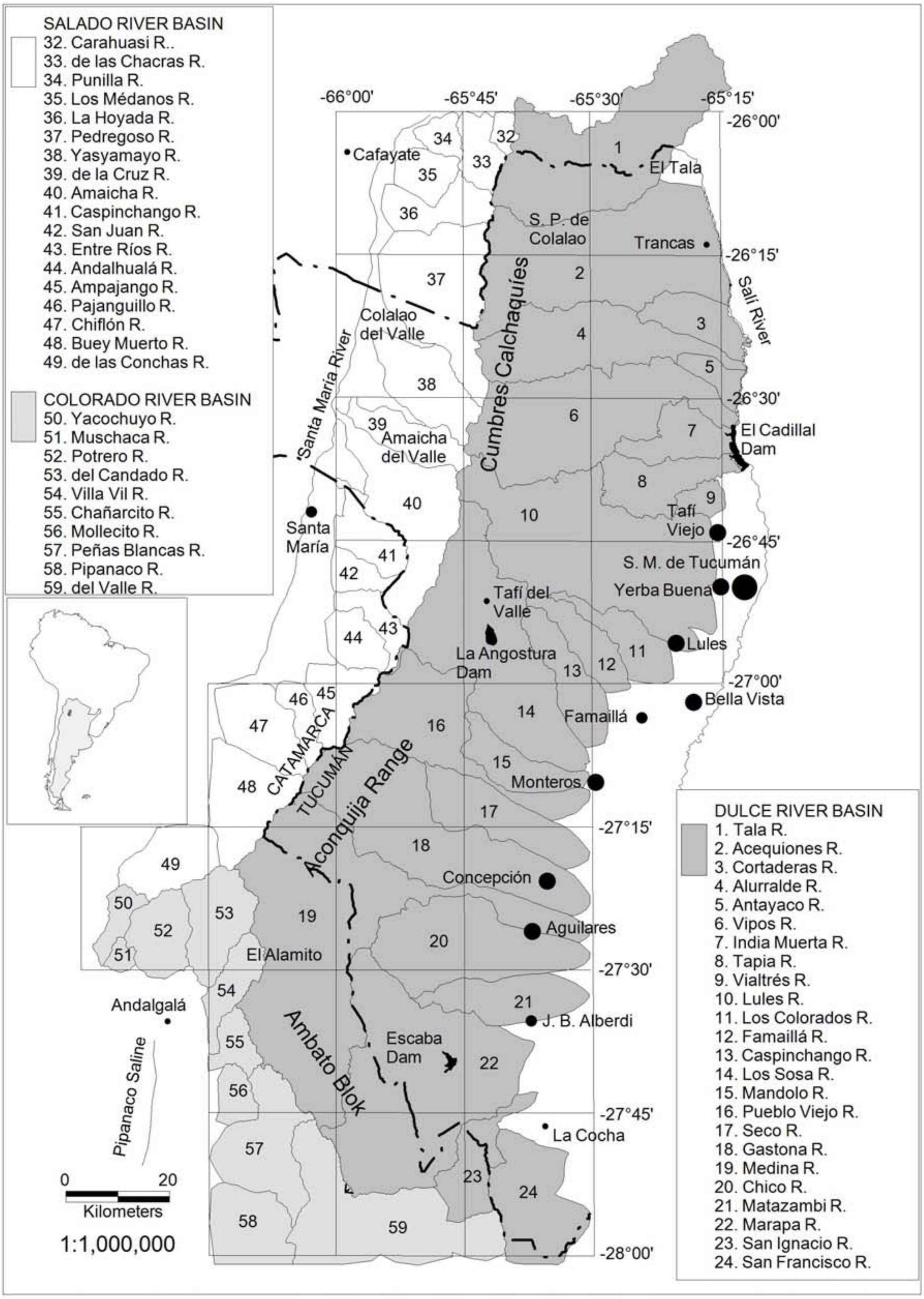


**Fig. 1 Map about hydro sub basin. The main river that gives name to the basin is identified with numbers. Population symbols represent the number of inhabitants per district: < 22,000; 22,000 a 50,000 a 110,000; and > 500,000.**

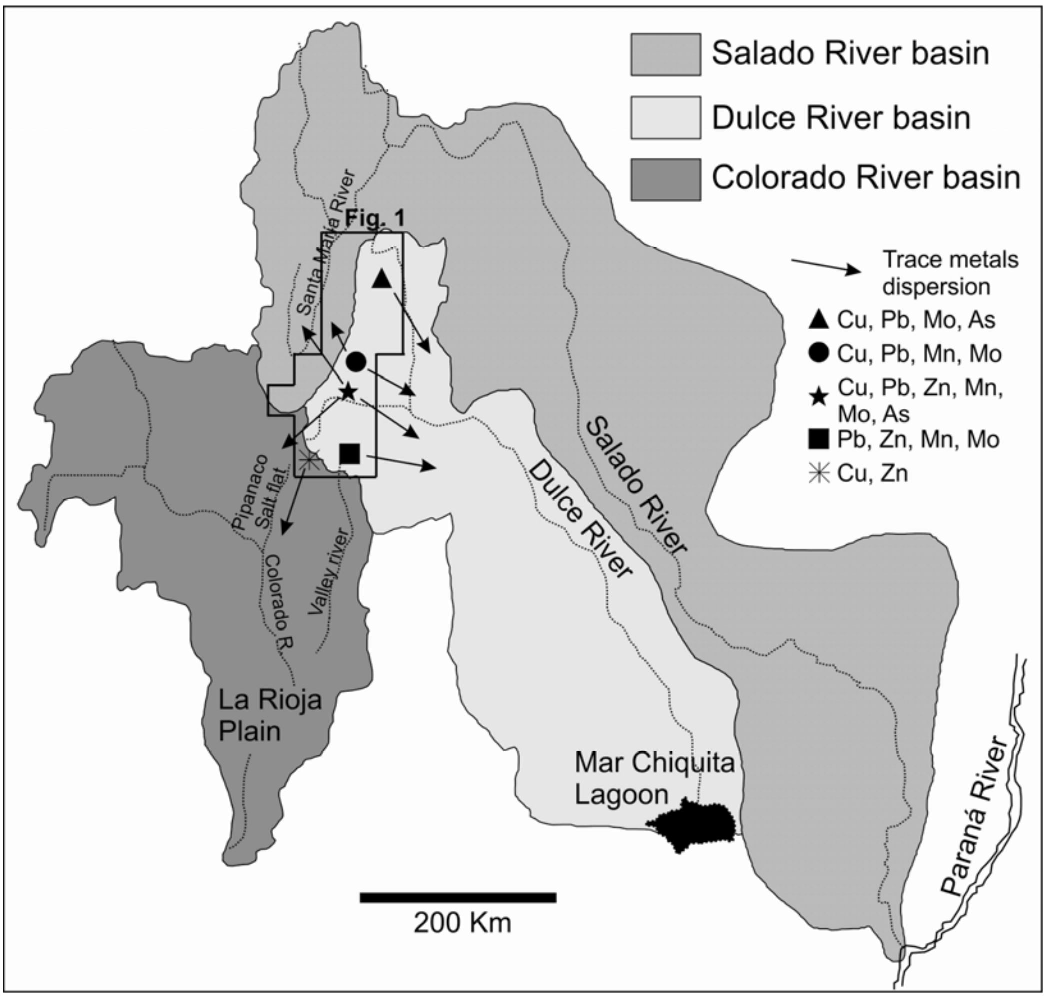


**Fig. 2 Map about location study area in relation to Salado, Dulce and Colorado rivers basins which flow into Paraná River, Mar Chiquita Lagoon and La Rioja plains, respectively.**

agricultural and urban area environments. Our work provides insights into the knowledge of the geochemistry distribution and concentration of elements Cu, Pb, Zn, Mn, Mo, As in stream sediment, constituting a contribution to environmental baseline studies, not performed in the area so far. Trace metals which are mainly transported by superficial drainage, are adsorbed on the soil components, reach people through crops or water consumption and high concentrations cause health affections. For example, population on the southeastern area of the Tucuman province, to where converge all drainage draining from the eastern sector of Cumbres Calchaquíes, Aconquija Range and Ambato Block, consumes water with high levels of As which are later on reflected in skin illnesses [1].

## 2. Methodology

In the 70s, the National Mining Secretary carried out the geochemical prospecting in the northwestern region of the country, obtaining fine chemicals stream sediments of the elements Cu, Pb, Zn.

In 2001, through an agreement between the Secretary of Mining of the Nation and the JICA (Japanese International Cooperation Agency), new chemical analyses about 34 elements have been done, which resulted in the publication, among others, of Multielements Geochemical Maps San Miguel de Tucumán, Concepción and Belén [2, 3]. To determine As, Instrumental Neutronic Activation methodology

was used and to determine elements Cu, Mn, Mo, Pb, Zn Spectroscope Emision Athomic-Induction joined to Plasma (EEA-ICP) of fragment < 80 mesh [4]. Detection limits of chemical tests were: Cu (0.5 ppm), Pb (2.0 ppm), Zn (0.5 ppm), Mn (1 ppm), Mo (1 ppm) and As (0.5 ppm).

14,976 geochemical data about stream sediments of Cu, Pb, Zn, Mn, Mo and As elements have been studied and obtained from Multi-element Geochemical Maps San Miguel de Tucumán, Concepción and Belén [2, 3]. Data were analyzed by multivariate geostatistical methods and correlated with the outcropping geological units and existing mineral manifestation, taking into account superficial draining network and hydric sub basin, which helps to determine the contribution and influence area about town population [5, 6]. For each element, outliers and external geochemical value have been determined. Outlier's values were removed from the data base because they present specific anomalies which distort subsequent geostatistical results.

The As and Mo elements have concentrations which are below the detections limits. Considering elements as As and Mo, whose lower detection limit geochemical data exceeded 70% of the total amount, were also removed from geostatistical treatment.

Thematic maps were prepared from the interpretation of Landsat and ASTER satellite images. The sampling sites were located on the draining map according to the locations that these were in original Mosaics of SEGEMAR (Geology and Mining Secretary of Argentina), so that each sample geographical coordinates have been obtained and geo-referred base chemical data was prepared.

## 3. Trace Metal Source

The basis of the geological sequence is represented by Upper Precambrian-Lower Cambrian metamorphic rocks age, which were intruded by granitic rocks during the Carboniferous and Ordovician Period. The igneous-metamorphic rock basement is covered by Cretaceous-Tertiary sediments and in some area volcanic and sub volcanic rocks, mainly from Tertiary Period, outcrop. With the intrusive rocks, veined mineralization and copper porphyry type are associated in some cases [5] (Fig. 3).

The present morphology of the mountains and the NW-SE and NE-SW major structures where originated mainly by the tectonic activity that has worked in the region since Tertiary and continues nowadays. The igneous activity in the Lower Paleozoic and Tertiary, together with tectonic processes, led to the location of mineral deposits and mineral manifestations in the area (Fig. 3). The mineralization is represented by gold and silver vein deposits and by copper-gold-molybdenum porphyry type deposits, mainly.

The gradual raising of mountain ranges to over 5,500 masl, the intense rock fracturing and high rainfall have produced an intense superficial alteration in rocks, which in some cases reaching to 10 m depth. In that way, the minerals that make up rocks were leached and transported into deep aquifers by the superficial drainage or through rock fracturing.

## 4. Geochemical Element Behavior

On the superficial environments, elements which are free from their primary structure are transported by different physical agents in the environment to form new secondary minerals, adsorbed by clays and oxides in stream sediments, in close relation with environmental pH and Eh. Some elements are also dispersed in a mechanic way like Au, which is transported as native gold. In other cases, the element mobility does not depend on environmental pH and the presence of other elements or compound limits its mobility. This is the case of Mo whose mobility in oxidizing environments is high, but it is low in reducing environments, restricted by the presence of Pb, Fe and carbonates. Elements Ag, Cu, Pb, Zn, Mn and As have different behavior whether the environment is oxidizing or reducing and, besides, each

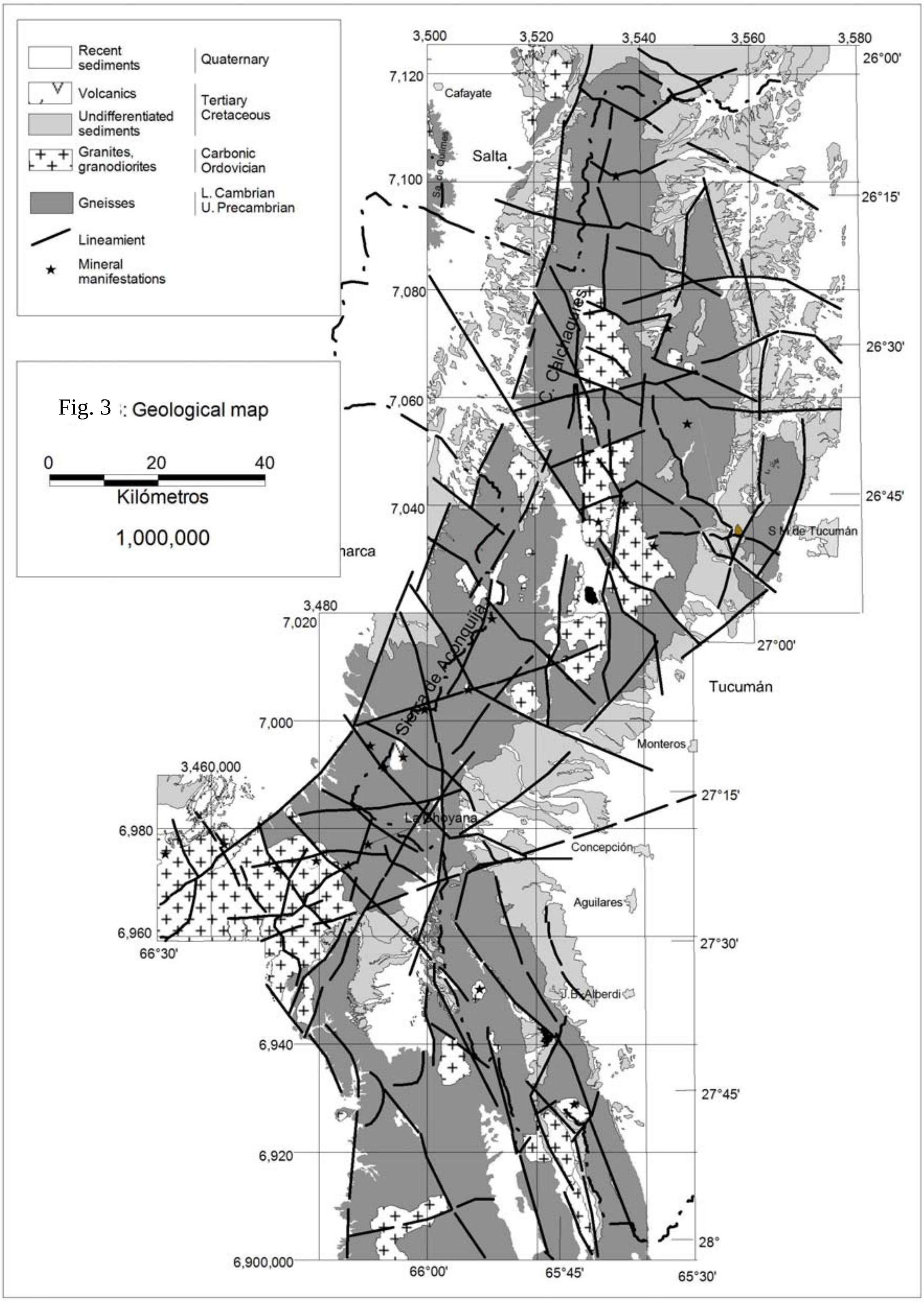


**Fig. 3 Generalized geological map. Big geological units, major structure bed deposits and mineral manifestations are indicated.**

of them precipitates at a different pH (Ag: 7.5-8.0; Cu: 5.3; Pb: 6.0; Zn: 7.0; Mn: 8.5-8.8) [7, 8].

The release of the elements are produced by chemical weathering in the presence of abundant water, $CO_2$, $O_2$, low temperature and pressure, or by physical weathering in desert environments and in cold, polar places; both types of weathering are favored by biological agents. Weathering reactions include hydrolysis and oxidizing. Hydrolysis is the reaction between water and the acid ion or a weak base; usually rainwater in equilibrium with $CO_2$ from the atmosphere have pH 5.7 and quickly attacks silicates and carbonates, releasing trace elements ($Fe_2SiO_4 + 4H_2O = 2Fe^{2+} + 4OH^- + H_4SiO_4$). Oxidizing produces gossans and Mn and Fe oxides when silicates are in contact with air or water ($2Fe_2SiO_4 + O_2 + 4H_2O = 2Fe_2O_3 + 2H_4SiO_4$) [7, 8].

Geochemical elements dispersion and geochemical associations in the secondary environment depend, among other factors, on the metals mobility, geochemical affinity and environment conditions. Meanwhile, there are many factors involved in the metal-mobility (nature of the environment, transport mechanisms, microorganism, salt solubility, complex ions, dissolved gases presence, permeability, porosity, grain size, etc.) and iron and manganese oxides have great capacity to absorb or coprecipitate most elements.

## 5. Conclusions

The ppm highest average geochemical concentrations are Cu: 28; Pb: 27; Zn: 97; Mn: 817; Mo: 2 and As: 14 (Fig. 4).

The high average geochemical concentrations of element Cu, Pb and Mo are spatially correlated in some sectors. In Cumbres Calchaquies and Aconquija Ranges, high concentrations of Cu, Pb and Mo occur in different areas with outcropping of Paleozoic intrusive rocks and known mineral manifestations.

In Ambato Block, high concentrations of Cu in the western side match up with outcropping of Paleozoic intrusive rocks and on the eastern side the highest concentrations of Pb are related to outcropping of Paleozoic intrusive rocks and known mineral manifestations (Figs. 4a-4c). The highest mean Zn and Mn are observed in the south side of Aconquija Ranges and in Ambato Block, related to Paleozoic intrusive rocks and known mineral manifestations (Figs. 4c-4d).

High concentrations of As and Mo on the eastern side of the Cumbres Calchaquíes have no relations to outcropping rocks and not known in the area mineral manifestation; however, at the southern end area of Aconquija Ranges, they are related to mineralized areas, Paleozoic and Tertiary intrusive rocks (Figs. 4e-4f).

Main geochemical associations were determined with the factor analyses. In the first factor, the most frequent geochemical association is represented by Cu-Zn-Mn elements, which would be adsorbed or precipitated by Mn oxides. In some areas, Pb, As and Mo are part of this compound. Other less frequently compounds in the first factor (Pb-Zn and Mn-As) and second (Mo-As) and third (Pb-Mo) factor, can be absorbed by other agents (clay, Fe and Al oxides and organic matter).

The compound resulted from Cu, Zn and Mn elements have its origin in metamorphic and granitic rocks outcrop in the whole area, but other compounds are related with mineralized areas and intrusive rocks. The Mo-As compound coincides with mineral manifestations in Ambato Block and, in Cumbres Calchaquíes it occurs over the outcropping of Paleozoic granitic rocks.

In Cumbres Calchaquíes the Pb-Mo compound is related to mineral manifestations, with Paleozoic granitic rocks and Tertiary sub volcanic intrusive rocks. In Ambato Block and Aconquija Range the Pb-Mo association coincides with the outcropping of Palaeozoic granite rocks and mineral manifestation.

Given the spatial distribution of geochemical higher average concentrations of the elements and superficial drainage (Figs. 1, 2 and 4), in Cumbres Calchaquíes

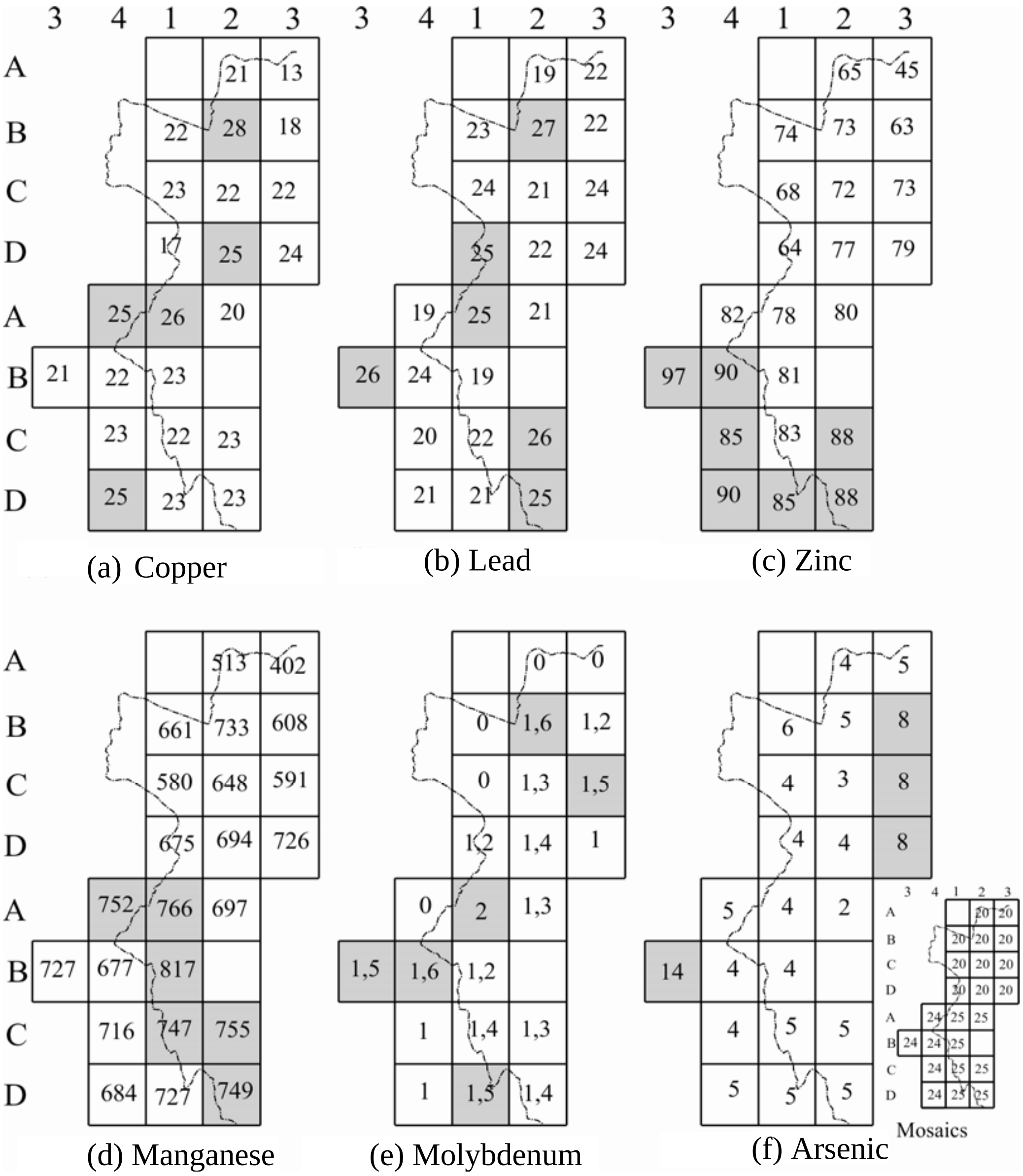


**Fig. 4 Map about the distribution of average geochemical concentrations with location in each mosaic. Geostatistic treatment about geochemical data was done by mosaic individually. Numbers represent the average concentrations in ppm, for example average concentrations of Cu in Mosaic Lo-Az is 21 ppm.**

Cu, Pb, Mo and As elements would be mainly transported to the east. In Aconquija Range Cu, Pb, Mn, Mo, in the northern area and Cu, Pb, Zn, Mn, Mo, As elements in the southern area would have any influence on the three main collectors (Santa María River, Pipanaco Salt flat and Salí River). The superficial drainage in Ambato Block distributes in solution Pb, Zn, Mn and Mo elements to Salí River and Cu, Zn elements to the South, to Colorado River basin.

## Acknowledgments

This project was supported by the CIUNT 26/G421. The manuscript has benefited from constructive comments of the reviewers.

## References

[1] R.S. Guber, L. Tefaha, N. Arias, N. Sandoval, R. Toledo, M. Fernández, et al., Contenido de arsénico en el agua de consumo en Leales y Graneros (Provincia de Tucumán-Argentina), Acta Bioquímica Clínica

Latinoamericana 43 (2) (2009) 201-207.

[2] L. Ferpozzi, A. Turel, D. Vargas, H. Valladares, A. Jara, D. Siehankiewicz, et al., Multi-element geochemical data and location of sampling sites of river sediment NOA I Geological-Mining Plan, Map 2766-III Belén, Catamarca province, Argentina Republic 2002, Institute of Geology and Mineral Resources, National Geological Mining Service, Buenos Aires, 2002.

[3] L. Ferpozzi, A. Turel, D. Vargas, H. Valladares, A. Jara, D. Siehankiewicz, et al., Multi-element geochemical data and location of sampling sites of river sediment NOA I Geological-Mining Plan, Map 2766-II San Miguel de Tucumán, Tucumán, Salta, Santiago del Estero and Catamarca provinces, Argentina Republic 2004, Institute of Geology and Mineral Resources, National Geological Mining Service, Buenos Aires, 2004.

[4] L. Ferpozzi, A. Turel, D. Vargas, H. Valladares, A. Jara, D. Siehankiewicz, et al., Multi-element geochemical data and location of sampling sites of river sediment NOA I Geological-Mining Plan, Map 2766-III Concepción, Catamarca, Santiago del Estero and Tucumán province, Argentina Republic 2003, Institute of Geology and Mineral Resources, National Geological Mining Service, Buenos Aires, 2003.

[5] A.A. Gutiérrez, Dispersión geoquímica secundaria de los elementos trazas en las sierras Calchaquíes, Aconquija y bloque Ambato, provincias de Tucumán y Catamarca, Ph.D. Thesis, Facultad de Ciencias Naturales e IML de la Universidad Nacional de Tucumán, 2009.

[6] A.A. Gutiérrez, R. Mon, R.N. Alonso, Inventory of traza elements as it bases for environmental studies, Tucumán and Catamarca, Argentina, in: 3rd Hemispheric Conference on Medical Geology, Montevideo, Uruguay, 2009.

[7] A.A. Levinson, Introductions to Exploration Geochemistry, Vol. 64, Applied Publishing Ltd. Representation, Economic Geology, Wilmette, Illinois, 1980, pp. 1-923.

[8] A.W. Rose, H.E. Hawkes, J.S. Webb, Geochemistry in Mineral Exploration, 2nd. Academic Press, New York, 1970, pp. 1-657.

Journal of Earth Science and Engineering 4 (2014) 121-125

# The Importance of Hunting and Hunting Areas for Big and Small Game (Food) for the Tourism Development in the Crna River Basin in the Republic of Macedonia

Cane Koteski, Dushko Josheski, Zlatko Jakovlev, Snezana Bardarova and Mimoza Serafimova

*Faculty of Tourism and Business Logistics, Goce Delchev University of Stip, Gevgelija 1480, Republic of Macedonia*

Received: December 20, 2013 / Accepted: January 20, 2014 / Published: February 25, 2014.

**Abstract:** The Crna River is a river in the Republic of Macedonia, right tributary to Vardar. Its source is in the mountains of Western Macedonia, west of Krusevo. It flows through the village of Sopotnica, and southwards through the plains east of Bitola. The name means "black river" in Macedonian, which is translation for its former Thracian name. The purpose of this paper is to show the hunting and hunting areas for big and small Game (food), the structure of the areas of certain hunting, fishing, fishing water objects, fish species, fishponds up to 20 years shown by municipalities and individual farms with ponds in the basin of Black River. It had used statistical data for the hunting grounds by areas, fishing ponds. Fish is very diverse in this river. Hunting in the Black River basin is of great importance for the economy of Republic of Macedonia. It is also a necessary factor for development of other economic activities.

**Key words:** Structure of the hunting grounds, fishing water objects, types of fish, fishponds, agricultural holdings.

## 1. Introduction

Hunting in the Crna River basin is presented as a branch in the economy, having in mind that special economic fundamentals are being made of each hunting area for the researched region, so one could feel free to point out that hunting includes: breeding, protection and exploitation of the Game (food) [1]. The useful part of hunting is that besides the production of meat and skins, it also creates conditions for development of other economic activities. It should be primarily mentioned the role of recreational sport hunting and its significance for the development of hunting tourism [2].

An important element in the analysis of hunting represents the total areas of the hunting grounds, so the data from Table 1 will be used.

**Corresponding authors:** Dusko Josheski, master, research field: economic geography. E-mail: dusko.josevski@ugd.edu.mk.

## 2. Materials

Fishing in the Black River basin has more sports-recreational character in the rivers and more economic-economic character in fishponds. Take care of stocking the river water objects that belongs to the sports fishing associations, such as Mamec from Prilep, Kajmakcalan from Bitola and all other fishing associations from other community centers, from Hisar, Krushevo, Dolneni, Novaci, Mogila and Tikvesh [3].

There are no written records about how much water fish stocks and micro accumulations in the rivers because fishing has no commercial and economic character except for the ponds, but the fact is that certain water objects have large quantities of fish such as rivers: Crna, Buturica, Lisicka, Gradeska, Belica, Konjarka, Satoka, Blato, Stroska and Golema [4]. Also all the micro accumulations on the territory from Black River basin are more or less fish stocked. The

**Table 1 Structure of the areas of certain hunting grounds in the Basin of Crna River for the period 1998-2007.**

| Area in ha | Hunting areas in the basin of Crna Reka | | | | | | | | | Total area in ha |
|---|---|---|---|---|---|---|---|---|---|---|
| | Hunting ground Veprcani 2001-2010 | Hunting ground Vitolishte 2001-2010 | Hunting ground Dunje 2001-2010 | Hunting ground Krushevica 2001-2010 | Hunting ground Melnica 2001-2010 | Hunting ground Trojaci 2001-2010 | Hunting ground Nidje 1998-2007 | Hunting Ground Staravina 1998-2007 | Hunting ground Strovija (Kadica) | |
| Total area Hunting ground | 6,200 | 15,028 | 8,730 | 6,300 | 8,780 | 7,670 | 22,003 | 10,960 | 11,034 | 85,671 |
| Hunting ground | 6,050 | 14,418 | 8,460 | 6,170 | 8,560 | 7,500 | 22,003 | 10,630 | 10,634 | 83,791 |
| Hunting productive area | 4,650 | 11,413 | 6,980 | 5,670 | 7,920 | 7,290 | 16,564 | 9,860 | 7,556 | 70,347 |
| Plough area | 683 | 1,495 | 1,761 | 2,659 | 1,526 | 1,650 | 802 | 1,881 | 1,972 | 12,457 |
| Meadows and pastures | 3,747 | 5,000 | 5,027 | 2,981 | 4,222 | 3,460 | 5,440 | 3,723 | 1,964 | 33,600 |
| Wood | 220 | 4,918 | 192 | 30 | 2,172 | 2,180 | 10,322 | 4,256 | 3,620 | 24,290 |
| Hunting unproductive area | 1,400 | 3,005 | 1,480 | 500 | 640 | 210 | 5,439 | 770 | 3,078 | 13,444 |
| Rivers,canals | 110 | 84 | 160 | 64 | 58 | 100 | 50 | 30 | 26 | 656 |
| Other areas | 1,290 | 2,921 | 1,320 | 436 | 582 | 110 | 5,389 | 740 | 3,052 | 12,788 |
| Unhunting area | 150 | 610 | 270 | 130 | 220 | 170 | 0 | 330 | 400 | 1,880 |

Hunting Commercial Basics of hunting association Deer from Hisar for the hunting grounds: Leskovo, Zurce and Pribilci [3]; Hunting Commercial Basics of hunting association Deer from Krushevo for the hunting grounds, Aldanci, Ostrilci and Divjaci [4];
Hunting Commercial Basics of hunting association Kavadarci from Kavadarci for the hunting grounds Seskovo, Kumanicevo; Lukar, Mrezicko, Drenovo, Rosoman, and et al. in state property [5];
Hunting Commercial Basics of hunting association Mukos from Prilep for the hunting grounds: Strovija-Kadica, Krstec-Nikodin, Belovodica, Vitoliste, Melnica, Krusevica, and et al. [6];
Hunting Commercial Basics of hunting associations from Bitola and hunting association Kajmakcalan from Staravina, Zlokukani, Sekirani, Sv Todori, Nidje and Staravina [7].

types of fish commonly fished in Black River basin are: catfish, carp, barbel or Gobio gobio, Carras, common bleak, common roach, Macedonian vimba, skobalt, perch, tench and trout [9].

One can conclude that the river water objects in the Black River basin are quite rich in diverse fish stocks, but one must point out for the selfless care of members of sport fishing association Mamec (Bait) from Prilep and Kajmakcalan from Bitola who regularly carried out fish stocking every year in the most of the water objects in the region investigated. The number of ponds in Black River basin is shown in Table 2.

## 3. Results and Discussion

According to data from the Table 2, it can be seen that in the Black River basin there are 22 individual farms with fishponds, they have a total of 23 fish ponds of which 19 are older than 20 years. Ponds cover a total area of 53,883 $m^2$, with a total volume of 391,743 $m^3$. Seen by municipalities, there are most ponds in the municipalities of Bitola and Kavadarci [10]. The number of households that own fish pond is 25 ha with a total area of 236 ha, of which for trout there are 65 ha, 147 ha for carp and other fish 123 ha. As to the capacity of the fishponds for trout, it is about 3,382 $m^3$; the carp is 115,462 $m^3$ and 268,478 $m^3$ for other fish [11].

It can be concluded that in future much more individual farmers should pay attention to the opening of new fishponds and fish stocking of rivers that has great importance for tourism development in the basin of Black River [12]. Also, in Table 3 are presented data about the area and the capacity of the fishponds.

In the Fig. 1, it is presented fishpond in the near village Babino.

## 4. Conclusions

Hunting in the Black River basin is presented as a branch, hunting includes: breeding, protection and exploitation of the game [13]. The hunt is not only for

**Table 2 Displaying fishponds in municipalities with up to 20 years and individual farms with ponds in Black River basin in 2007.**

| Municipality | Individual farmholds with objects (fishponds) | Fishponds | | Fishponds | |
|---|---|---|---|---|---|
| | | Total number | From which up to 20 years | Area ($m^2$) | Volume ($m^3$) |
| Bitola | 3 | 4 | 3 | 40,990 | 361,980 |
| Gradsko part of the basin | 0 | 0 | 0 | 0 | 0 |
| D.Hisar | 1 | 1 | 1 | 300 | 600 |
| Dolneni | 2 | 2 | 2 | 205 | 525 |
| Drugovo part of the basin | 3 | 3 | 2 | 1,500 | 1,800 |
| Kavadarci part of the basin | 4 | 4 | 4 | 3,280 | 5,690 |
| Krivogastani | 1 | 1 | 1 | 600 | 7,200 |
| Krusevo | 0 | 0 | 0 | 0 | 0 |
| Mogila | 0 | 0 | 0 | 0 | 0 |
| Novaci | 0 | 0 | 0 | 0 | 0 |
| Prilep | 7 | 7 | 6 | 6,980 | 13,892 |
| Rosoman | 1 | 1 | 0 | 28 | 56 |
| Caska part of the basin | 0 | 0 | 0 | 0 | 0 |
| Total | 22 | 23 | 19 | 53,883 | 391,743 |

**Table 3 Area and capacity of the fishponds in 2007**

| Municipalty | Nr of households that have fishponds | Surface of the fishponds (ha) | | | | Capacity of fishponds ($m^3$) | | |
|---|---|---|---|---|---|---|---|---|
| | | Total | For trout | For carp | For other fish | For trout | For carp | For other fish |
| Bitola | 6 | 4.13 | 0.03 | 1.15 | 2.95 | 630 | 96,480 | 265,500 |
| Gradsko part of the basin | 0 | 0 | 0 | 0 | 0 | 0 | 0 | 0 |
| Hisar | 1 | 0.30 | 0.30 | 0 | 0 | 0 | 0 | 0 |
| Dolneni | 1 | 0.01 | 0 | 0.01 | 0 | 0 | 150 | 0 |
| Drugovo part of the basin | 2 | 0.20 | 0.20 | 0 | 0 | 1,540 | 0 | 0 |
| Kavadarci part of the basin | 5 | 0.38 | 0.12 | 0.23 | 0.03 | 1,200 | 6,340 | 650 |
| Krivogas | 1 | 0.60 | 0 | 0.60 | 0 | 0 | 7,200 | 0 |
| Krushevo | 0 | 0 | 0 | 0 | 0 | 0 | 0 | 0 |
| Mogila | 0 | 0 | 0 | 0 | 0 | 0 | 0 | 0 |
| Novaci | 1 | 0.00 | 0.00 | 0 | 0 | 12 | 0 | 0 |
| Prilep | 7 | 0.70 | 0 | 0.47 | 0.23 | 0 | 5292 | 2300 |
| Rosoman | 1 | 0.00 | 0 | 0 | 0.00 | 0 | 0 | 28 |
| Caska part of the basin | 0 | 0 | 0 | 0 | 0 | 0 | 0 | 0 |
| Total | 25 | 236 | 65 | 147 | 123 | 3,382 | 115,462 | 268,478 |

Inventory of R. Makedonija 2007; Skopje 2008; Calculations from the author.

production of meat and skins, it creates conditions for development and other economic activities. This primarily have to be mentioned the role of recreational sport hunting and its significance for the development of hunting tourism [14]. An important element in the analysis of hunting is the total areas of the hunting grounds. Major commercial hunting areas that exist in Crna reka basin are:

(1) Hunting Commercial Basics of hunting association Deer from D. Hisar for the hunting grounds: Bazernik, Leskovo, Zurce and Pribilci;

(2) Hunting Commercial Basics of hunting association Deer from Krushevo for the hunting grounds Aldanci, Ostrilci and Divjaci;

(3) Hunting Commercial Basics of hunting association Kavadarci from Kavadarci for the hunting grounds Seskovo, Kumanicevo, Lukar, Mrezicko, Drenovo, Rosoman, Marena Vatasha, Koshani, Cemersko and Klinovo-Rozden in state property;

**Fig. 1 Fishpond in the near of v. Babino (Aug. 24, 2008).**

(4) Hunting Commercial Basics of hunting association Mukos from Prilep for the hunting grounds: Strovija-Kadica, Krstec-Nikodin, Vitoliste, Melnica, Krusevica, Dunje, Prilepec, Podmol, Erekovci, Topolcani, Zagoreska korija, Sredorek, Krivogastani, Dolneni, Slavej, Oreovec, and Trojaci;

(5) LSO, Hunting Commercial Basics of hunting associations from Bitola and hunting association Kajmakcalan from S. Staravina: Zlokukani, Sekirani, SV Todori, Nidje and Staravina.

One can conclude that in the Black River basin there are excellent conditions for development of hunting tourism [15].

Fishing in Black River basin has sports recreational character in rivers and economic character in fishponds [16].

The fish stocking of river water objects is made by sports fishing associations, such as Mamec from Prilep, Kajmakcalan from Bitola and all other fishing associations from other community centers including Krusevo Dolneni Novaci, Mogila and Tikvesh [17].

Major water objects that possess large quantities of fish are the rivers: Crna, Buturica, Lisicka, Gradeska, Belica, Konjarka, Satoka, Blato, Stroska and Golema River [18].

All micro accumulations on the territory of the Black River basin are more or less fish stocked [19].

From the fish that is usually fished in the Basin of Crna River, they are: catfish, carp, barbel or gobio gobio, Carras, common bleak, common roach, Macedonian vimba, skobalt, Tench and trout [20]. River water objects in the Crna River basin are quite rich in diverse fish stocks, and they contribute much to the development of the weekend sport fishing tourism [21, 22].

## Reference


[1] I. Basevski, Prilep Lake, Geografski razgledi Scientific society Prilep 7, Skopje, 1969, pp. 78-89.

[2] M. Gasevski, Hydrographic features of Mariovo, Scientific Society, Prilep, 1984, pp. 22-28.

[3] G. Basevski, Trojachka valley, the natural conditions for development of hunting in Trojachka Valley, 1989, pp. 84-99, 127-135.

[4] D. Kolcakovski, Basic Biogeographic Features of Macedonia Geografski Razgledi Book, Skopje, 2000, p. 35.

[5] D. Kolcakovski, Nidje mountain (Kajmakcalan 2.520 m)—Basic geomorphologic features, 2004, pp. 110-115.

[6] C. Kotevski, Hydrological features of the basin of Crna River, 1971, pp. 123-128.

[7] C. Koteski, Thematic atlas of Mariovo and Raecka valley, Master work, Faculty of Geography, University of Skopje, 2004, pp. 201-205.

[8] B. Markoski, Cartographic definition and differentiation of mountain, 2005, pp. 101-105.

[9] Spatial entities in the Republic of Macedonia, Skopje, Bulletin for physical geography, 2rd, 2009, pp. 25-34, 201-207.

[10] I. Matanickin, Z. Pavletis, Life of Our Rivers, Zagreb, Geographical Studies, Skopje, 1972, pp. 151-155.

[11] M. Milosevski, M. Zlateski, Waterpower engineering in Pelagonia, Bitola field Status, Development and Perspective, Bitola, 1998, pp, 141-150.

[12] K. Micevski, Flora in R. Macedonia, MANU, Vol. 1, Skopje, 1993, pp. 70-74.

[13] N. Panov, Tourist valorization of the artificial lakes in R. Macedonia, Master work, Faculty of Geography, University of Skopje, Belgrad, 1998, pp. 22-23.

[14] N. Panov, Development of tourism in R. Makedonija, Zbornik, and First congress of geographers of R. Makedonija held in Ohrid od 26-28.10. 1995, Skopje, Makedonije, Forest encyclopedia, Vol. 3, Zagreb, 1996, pp. 24-25.

[15] V. Sokoloski, Microacumulations, Macedonian waterpower engineering, No. 10, Skopje, 1997, pp. 25-26.

[16] A. Stojmilov, Tourist value of the mountains in SR Makedonija, Annual Review of the Institute for Geography, No. 21, Skopje, 1975, pp. 45-47.

[17] A. Stojmilov, Spatial factors in development of tourism in Kozuf-Nidje region, Annual Review of Faculty for Geography, University of Skopje, 1980, pp. 56-57.

[18] A. Stojmilov Forestry in Mariovo, Complex Geographical Studies, Faculty of geography, University of Skopje, 1984, pp. 201-202.

[19] Book of Ministry of Agriculture, Forestry and Water Economy R. Macedonia Hunting Ground Nr.1, Strovija-Prilep, Skopje, 2001, pp. 190-191.

[20] Book of Ministry of Agriculture, Forestry and Water Economy R. Macedonia, Hunting Ground Nr. 4, Nixe-Bitola, 1998-2007, Skopje, 1998, pp. 80-81.

[21] Ministry of Agriculture, Forestry and Water Economy R. Macedonia. Hunting Ground Nr. 5, Staravina-Bitola, Skopje, 1998, pp. 90-91.

[22] Book of Ministry of Agriculture, Forestry and Water Economy R. Macedonia Hunting Ground Nr. 4, Vitolishte-Prilep, Skopje, 2001, pp. 70-72.

Journal of Earth Science and Engineering
Volume 4, Number 2, February 2014

David Publishing Company
240 Nagle Avenue #15C, New York, NY 10034, USA
Tel: 1-323-984-7526, 323-410-1082; Fax: 1-323-984-7374, 323-908-0457
http://www.davidpublishing.com, www.davidpublishing.org
earth@davidpublishing.org, earth_science2011@hotmail. com

ISSN 2159-581X
02
9 772159 581143